O.A. YESHCHENKO,[1] A.O. PINCHUK[2]

[1] Taras Shevchenko National University of Kyiv, Physics Department
 (64/13, Volodymyrs'ka Str., Kyiv 01601, Ukraine; e-mail: yes@univ.kiev.ua)
[2] Department of Physics and Energy Sciences, University of Colorado at Colorado Springs
 (1420 Austin Bluffs Pkwy, Colorado Springs, Colorado 80933, USA)

THERMO-OPTICAL EFFECTS IN PLASMONIC METAL NANOSTRUCTURES

The effects of the temperature on the surface plasmon resonance (SPR) in noble metal nanoparticles at various temperatures ranging from 77 to 1190 K are reviewed. A temperature increase results in an appreciable red shift and leads to a broadening of the SPR in the nanoparticles (NPs). This observed thermal expansion along with an increase in the electron-phonon scattering rate with rising temperature emerge as the dominant physical mechanisms producing the red shift and broadening of the SPR. Strong temperature dependence of surface plasmon enhanced photoluminescence from silver (Ag) and copper (Cu) NPs is observed. The quantum photoluminescence yield of Ag nanoparticles decreases as the temperature increases, due to a decrease in the plasmon enhancement resulting from an increase in the electron-phonon scattering rate. An anomalous temperature dependence of the photoluminescence from Cu nanoparticles was also observed; the quantum yield of photoluminescence increases with the temperature. The interplay between the SPR and the interband transitions plays a critical role in this effect. The surface-plasmon involved laser heating of a dense 2D layer of gold (Au) NPs and of Au NPs in water colloids is also examined. A strong increase in the Au NP temperature occurs, when the laser frequency approaches the SPR. This finding supports the resonant plasmonic character of the laser heating of metal NPs. The sharp blue shift of the surface plasmon resonance in colloidal Au NPs at temperatures exceeding the water boiling point indicates the vapor-bubble formation near the surface of the NPs.

K e y w o r d s: metal nanoparticles, surface plasmon resonance, temperature effects, electron-phonon scattering, nanoparticle thermal expansion, plasmon enhanced photoluminescence, light-induced heating.

1. Temperature Effects on the Surface Plasmon Resonance in Metal NPs

1.1. Introduction

Noble metal NPs have attracted a considerable attention recently due to a wide range of potential applications in surface enhanced Raman scattering (SERS) [1–3], surface enhanced fluorescence [4–6], biochem-

ical imaging [7–9], cancer treatment [7, 10–12], and subwavelength optical waveguides [13–17] among others. Noble metal NPs exhibit unique optical properties which are not found in their bulk counterparts. In particular, those are the resonant absorption and light scattering [18, 19]. Collective coherent excitations of free electrons in the conduction band, also known as Surface Plasmon Resonance (SPR), are responsible for this strong absorption and the scattering of light by particles [18]. The energy and width of the SPR depend on the morphology, size, spatial ori-

entation, and optical constants of the particles and of the surrounding medium [18, 19].

Understanding the influence of the temperature on the SPR in metal NPs is crucial for both pure and applied sciences of the NPs [18, 22], considering recent applications of noble metal NPs in thermally assisted magnetic recording [23], thermal cancer treatment [12, 24–26] catalysis and nanostructure growth [27], and computer chips [28]. Additionally, understanding the underlying physics of the temperature dependence of optical properties of metal NPs is a precondition for the development of successful and reliable applications and devices. However, SPR temperature dependence has not been studied in great details to-date, primarily, because the creation of a broad temperature interval requires using materials with high thermal stability. Colloids, thin films, and glasses, which are major media in optical materials combined with metal NPs typically do not possess enough the thermal stability ($\sim$500–600 °C is the maximum range for glasses). The use of silica, a more advanced material, which is highly transparent in the optical range, along with the facile sol-gel technique allow the production of metal NPs of a distinct chemical nature and size range within the matrix stable in air up to 1300 °C. The use of silica sol-gel glasses allows studying the temperature effects on SPR in metal NPs in a wide temperature interval without the risk of a sample destruction.

The temperature effects for the SPR absorption band in metal NPs were studied by Kreibig [18, 29], Doremus [30,31], and the origin of temperature effects upon the SPR was analyzed by Mulvaney [32]. Recently, the influence of the temperature on the SPR in Au-based plasmonic nanostructures was described for low temperatures, from 80 to 400 K in Ref. [33], where an appreciable red shift and broadening of the SPR with increasing temperature were observed. The temperature-induced broadening of the SP absorption band led to an appreciable decrease in the light absorption at the frequency of the SPR and to an increase in absorption on the wings of the SP absorption band. The interplay between temperature effects and the material quality in nanoscale plasmonic wave guiding structures is discussed in Ref. [34]. Most of the effects relating to the temperature dependence of the SPR were observed for low temperatures [18, 33]. There is a lack of data on the influence of the temperature on the SPR in metal nanos-

tructures for temperatures higher than room temperature. Link and El-Sayed studied the temperature dependence of the SPR energy and bandwidth for Au colloidal NPs [35] at temperatures above room temperature. Au colloidal NPs within a size range of 9 nm up to 99 nm were studied at elevated temperatures up to 72 °C. No significant influence of the temperature on the SPR energy and bandwidth was discovered.

In our recent works [36–39], the temperature dependences of the SPR in the noble metal (Ag, Au, Cu) NPs of various sizes in a silica matrix have been studied at high temperatures. We observed that an increase in the temperature of the sample leads to a red shift and broadening of the SPR like the results of Bouillard *et al.* [33] obtained for Au nanostructures at low temperatures. The observed temperature dependence of the SPR has been analyzed within a theoretical framework, with a model considering such phenomena as the thermal volume expansion of a NP, electron-phonon scattering in the NP, and temperature dependence of the dielectric permittivity of a host matrix. We found that the primary cause for a red shift of the SPR with increasing temperature is the thermal volume expansion of the NP, while the electron-phonon scattering in the NP is the dominant mechanism of SPR broadening. Additionally, the full reversibility in a variation of optical characteristics for these samples was observed.

1.2. Synthesis and Structural Characterization of Noble Metal NPs in SiO$_2$ Matrix

Composite Me/SiO$_2$ samples (where Me is Ag, Au, and Cu) containing the noble metal NPs were produced using a modified sol-gel technique based on the hydrolysis of tetraethoxysilane (TEOS), with Au-doping followed by a chemical transformation of the dopant precursors annealing in air [36–42]. A precursor sol was prepared by mixing TEOS, water, and ethyl alcohol with acid catalysts HNO$_3$, HCl, or H$_2$SO$_4$. Silica powder (aerosol A-300) was then added to the sol and followed with the ultrasonication to prevent a large volume contraction during drying. The next step in the gelation process resulted in the formation of gels. This resulted in porous materials (xerogels), once the gels were dried at room temperature. The porosity of the SiO$_2$ matrices was controlled by annealing the samples in air at 600 °C
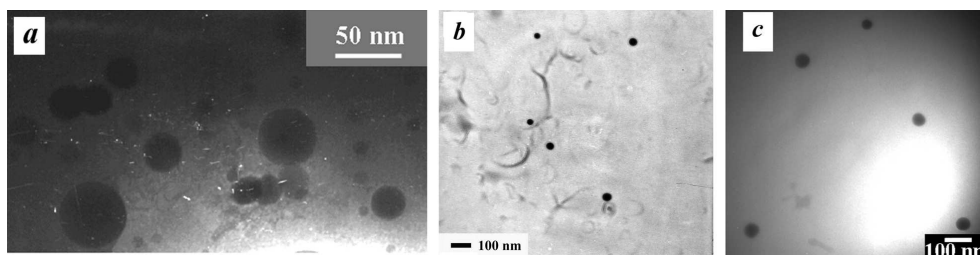
Fig. 1. TEM images of (*a*) Ag nanoparticles (mean size $\langle d \rangle = 30$ nm with standard deviation $\sigma_d = 13$ nm), (*b*) Au nanoparticles ($\langle d \rangle = 36$ nm with $\sigma_d = 5$ nm) and (*c*) Cu nanoparticles ($\langle d \rangle = 48$ nm with $\sigma_d = 7$ nm) in silica glass. (Modified from Refs. [36, 38, 40])

for a duration of 1 hour. Doping by Ag, Au, or Cu was performed by immersing the xerogels into an $AgNO_3$, $HAuCl_4$, or $Cu (NO_3)_2$ alcohol solution for 24 hours. Metal salt solutions of differing concentrations were then used. The metal-doped samples were air-dried and annealed with a gradual increase in the temperature from 20 °C to 1200 °C. The annealing was performed in an air or hydrogen atmosphere and resulted in the decomposition of a metal salt, followed by the nucleation and aggregation of metal clusters, finally resulting in the formation of metal NPs of various sizes. The higher the concentration of a metal salt used at the impregnation of xerogel during the doping step, the higher the optical density of the corresponding Me/SiO_2 final sample. The set of Ag/SiO_2, Au/SiO_2, and Cu/SiO_2 composite samples containing metal NPs of various sizes was fabricated, in that respective order.

These metal NPs were characterized with transmission electron microscopy (TEM) to determine their mean size and morphology. Figure 1 shows the typical micrograph of these samples. TEM provides the following mean sizes of metal NPs in fabricated Me/SiO_2 samples. For Ag NPs, the following was determined: $\langle d \rangle = 30$ nm with the standard deviation $\sigma_d = 13$ nm for the Ag1 set of samples, and $\langle d \rangle = 60$ nm with $\sigma_d = 12$ nm for the Ag2 set of samples. For Au NPs: $\langle d \rangle = 20$ nm with $\sigma_d = 3$ nm for the Au1 set of samples, $\langle d \rangle = 36$ nm with $\sigma_d = 5$ nm for the Au2 set of samples, and $\langle d \rangle = 55$ nm with $\sigma_d = 8$ nm for the Au3 set of samples. For Cu NPs: $\langle d \rangle = 17$ nm with $\sigma_d = 2$ nm for the Cu1 set of samples, $\langle d \rangle = 35$ nm with $\sigma_d = 5$ nm for the Cu2 set of samples, $\langle d \rangle = 48$ nm with $\sigma_d = 7$ nm for the Cu3 set of samples, and $\langle d \rangle = 59$ nm with $\sigma_d = 10$ nm for the Cu4 set of samples. TEM indicates the formation of spherical NPs with a large distance separating the NPs. Thus, the electrodynamical coupling cannot affect their optical features, enabling us to use one-particle models for the simulations below. Additionally, the TEM analysis shows that increasing the metal salt concentration leads to the formation of larger NPs, which agrees with the conventional understanding of the aggregation of metal NPs in solids. A tungsten-halogen incandescent lamp served as a light source for the measurements of absorption spectra. The samples were placed in an open furnace during the spectral measurements, and each spectrum was measured at its own respective stabilized temperature.

1.3. Temperature Dependence of Surface Plasmon Resonance in Noble Metal NPs: The Experiment

1.3.1. Au NPs in SiO₂ matrix

We measured the absorption spectra of Au NPs in a silica host matrix; samples containing Au NPs with a mean diameter of 20 nm, 36 nm, and 55 nm were studied, respectively. Absorption spectra were measured in the temperature range from 17 to 915 °C [37]. To the best of our knowledge, studies of the surface plasmon optical spectra in Au NPs in such a broad temperature range were performed for the first time. The goal was to examine the influence of the temperature on the spectral characteristics (energy and bandwidth) of SPR in Au NPs. The evolution of the experimental absorption spectrum of the composite sample containing Au NPs with a mean size of 20 nm is shown in Fig. 2. The total absorption spectra were fitted by basic Lorentzian bands, and the studied absorption spectra contain two bands, one high-energy band and one low-energy band. The high-energy band results from interband transitions in Au, and the low-energy

band is caused by the excitation of surface plasmons in Au NPs. Within the studied sample, the SP band falls in the spectral range of 2.17–2.32 eV, depending upon the NP size and temperature. Such spectral positioning of the SP band is typical of Au NPs embedded in silica [18]. The decomposition of spectra to Lorentzian bands allowed us to extract the SP band from the total spectrum and to determine its spectral position and bandwidth.

Figure 3 displays the obtained temperature dependence of the SPR energy and bandwidth for Au NPs of various sizes. Figures 2 and 3 illustrate that the increase in the temperature from 17 to 915 °C leads to a monotonous red shift (shift to lower frequencies) of the surface plasmon band and its significant broadening. Thus, the manifestations of the temperature effects on the surface plasmon resonance in Au NPs are quite prominent. Attained dependences are not qualitatively distinct for the Au NPs with distinct sizes in the studied size range. The absorption spectra of the studied Au/SiO$_2$ composite samples were measured at both heating and cooling. The full reversibility in the temperature behavior of the spectra was observed, indicative of a high thermal stability and of a high optical quality of sol-gel prepared Au/SiO$_2$ nanocomposites. This may be important for the application of such nanocomposites in optical devices working under extreme thermal conditions.

1.3.2. Ag NPs in SiO$_2$ matrix

Absorption spectra of Ag NPs with mean sizes of 24 nm and 60 nm in the silica host matrix were measured in the temperature range from 17 to 700 °C [38]. The evolution of the experimental absorption spectrum of the composite sample containing Ag NPs with a mean size of 24 nm is shown in Fig. 4. Again, the energy and width of SPR were determined by fitting the observed SP absorption band with Lorentzian bands. Here, the SP band is in the spectral range of 2.93–3.06 eV, depending on the NP size and temperature. Such spectral positioning of the SP band is typical of Ag NPs embedded in silica [18].

Figure 5 shows the attained temperature dependence of the SPR energy and bandwidth for the Ag NPs of various sizes. Figures 4 and 5 show that the increase in the temperature from 17 to 700 °C also leads to a monotonous red shift of the SPR band and its broadening. The obtained dependences are
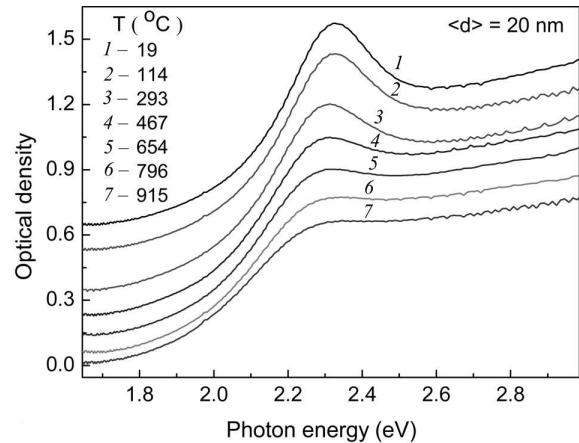
Fig. 2. Evolution of the experimental absorption spectrum of Au nanoparticles with a mean size of 20 nm in silica with the gradual increase in the temperature from 19 to 915 °C. (Modified from Ref. [38])
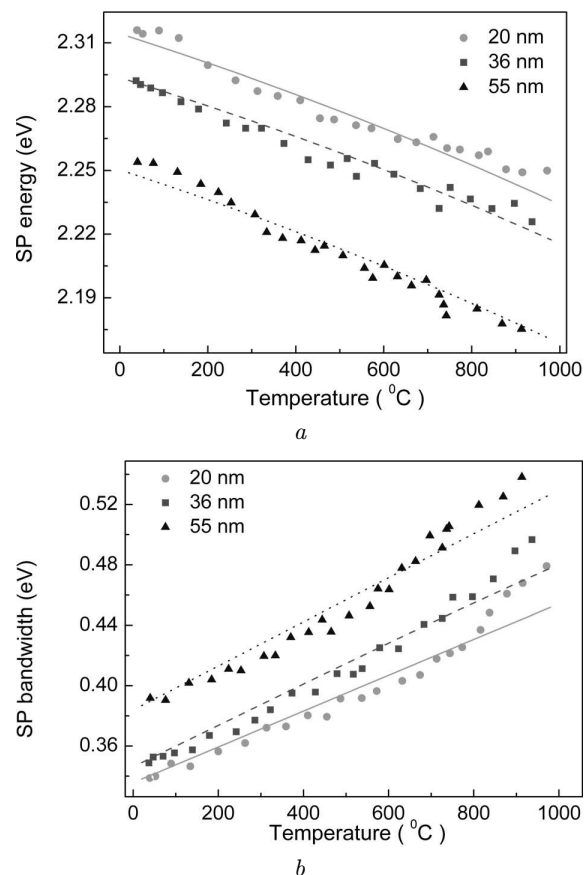
Fig. 3. Dependences of the SPR energy (*a*) and bandwidth (*b*) for gold nanoparticles of various sizes in silica. Dots – experiment, lines – theory. (Modified from Ref. [38])
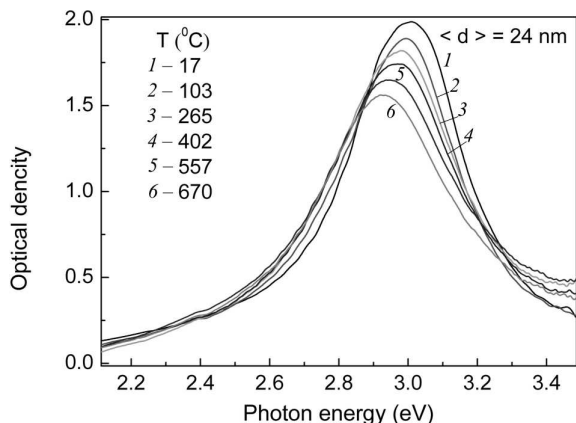
Fig. 4. Evolution of the experimental absorption spectrum of Ag nanoparticles with a mean size of 24 nm in silica with a gradual increase in the temperature from 17 to 670 °C. (Modified from Ref. [37])
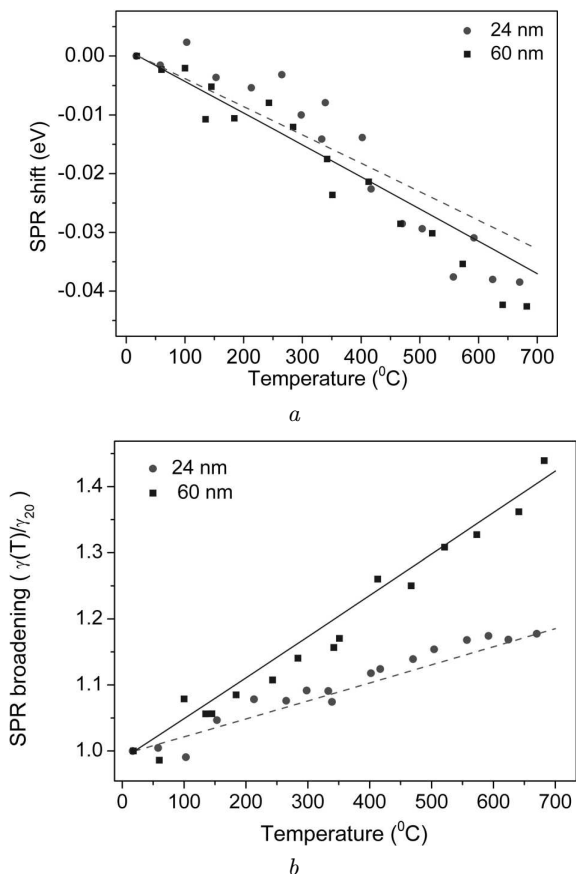

a

b

Fig. 5. Dependences of the SPR energy (*a*) and band width (*b*) for silver NPs of various sizes in silica. Red circles and dashed line – 24 nm NPs, blue squares and solid line – 60 nm NPs. Dots – experiment, lines – theory. (Modified from Ref. [37])
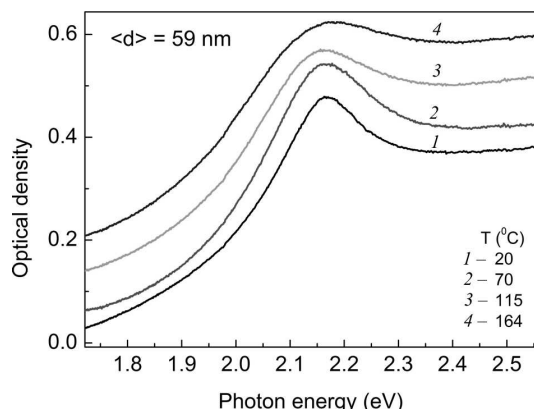

Fig. 6. Evolution of the experimental absorption spectrum of Cu nanoparticles with a mean size of 59 nm in silica with a gradual increase in the temperature from 20 to 164 °C. (Modified from Ref. [39])

not qualitatively different for Ag NPs of different sizes. The observed temperature dependences for Ag NPs in silica are similar to those observed for Au NPs in the same host matrix (see subsection 1.3.1 and Ref. [37]). For example, both exhibit the red shift and broadening of SPR with increasing temperature. Let us note that, similarly to the Au/SiO_2 composite samples, the absorption spectra of Ag/SiO_2 composite samples are fully reversible under many cycles of heating and cooling. Once again, this may find use in applications in optical devices working under extreme thermal conditions.

1.3.3. Cu NPs in SiO_2 matrix

Finally, the absorption spectra of Cu NPs with a mean size of 17 nm, 35 nm, 48 nm, and 59 nm in a silica host matrix were studied in the temperature range from 20 to 187 °C [39]. The evolution of the experimental absorption spectrum of the composite sample containing Cu NPs with a mean size of 59 nm is shown in Fig. 6. The absorption spectra, which contain two bands, were fitted by Lorentzian spectral bands. Like in the Au experiment, the high-energy band is caused by the interband transitions in Cu, and the low-energy band results from the excitation of surface plasmons in Cu NPs. For the studied samples, the SP band is in the spectral range of 570 nm (2.18 eV)–580 nm (2.14 eV), again depending on the NP size and temperature. Such spectral position of the SP band is typical of Cu NPs embedded in silica [18].

116

Figure 7 presents the temperature dependence of the SPR energy and bandwidth for the Cu NPs of various sizes. Figures 6 and 7 show that, just as in the Au experiment, the increase in the temperature from 293 to 460 K leads to a monotonous red shift of the surface plasmon band and its broadening. Manifestations of the effects of the temperature on the SPR in Cu NPs are quite prominent. As with the Ag NPs, the obtained dependences are not qualitatively different for the Cu NPs of various sizes in the studied size range. Thus, the observed temperature dependences for Cu NPs in silica are quite similar to those observed for Ag [36, 38] and Au [37] NPs in the same host matrix, again as seen by the red shift and broadening of SPR with increasing temperature.

Once more, the absorption spectra of the studied Cu/SiO$_2$ composite samples were measured at both heating and cooling, and once more the full reversibility of the temperature behavior of the spectra was observed. This indicates a high thermal stability and a high optical quality of sol-gel prepared CuSiO$_2$ nanocomposites, which is again important for the same aforementioned applications.

1.4. Temperature Dependence of Surface Plasmon Resonance in Metal NPs: Theory

This section provides a theoretical analysis of the various mechanisms that produced the observed temperature effects; this is the theoretical analysis of the causes for the red shift and broadening of SPR in metal NPs occurring with an increase in the temperature. Those effects are rooted in the following: (1) electron-phonon scattering in the NP, (2) thermal expansion of the NP and (3) temperature dependence of the dielectric permittivity of the silica host matrix.

It is well known (see Refs. [18, 19]) that the absorption coefficient of the composite material, containing the non-interacting spherical metal NPs much smaller than the light wavelength ($d \ll \lambda$), is

$$\kappa(\omega) = \frac{9f\omega\varepsilon_m^{3/2}}{c} \frac{\varepsilon_2}{(\varepsilon_1 + 2\varepsilon_m)^2 + \varepsilon_2^2}, \tag{1}$$

where ω is the frequency, c is the light velocity, $\varepsilon(\omega) = \varepsilon_1(\omega) + i\varepsilon_1(\omega)$ is the dielectric permittivity of NP, f is the filling factor of the composite, and ε_m is the dielectric permittivity of the host matrix. The temperature dependence of the permittivities of NP and the host matrix would affect the energy and
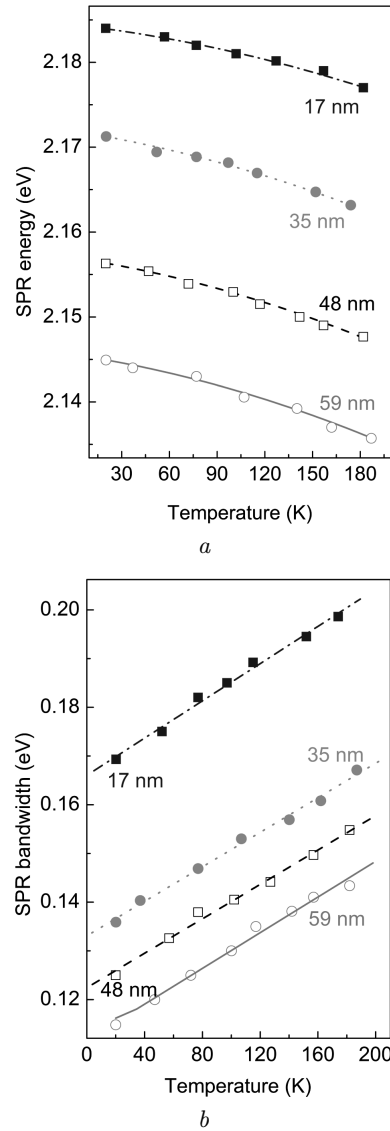

Fig. 7. Dependences of the SPR energy (*a*) and bandwidth (*b*) for copper nanoparticles of various sizes in silica. Dots – experiment, lines – theory. (Modified from Ref. [39])

width of SPR within the NP and would, correspondingly, affect the absorption spectrum of the composite. The dielectric permittivity of a metal can be expressed as

$$\varepsilon(\omega) = \varepsilon_{ib}(\omega) + \varepsilon_D(\omega), \tag{2}$$

where $\varepsilon_{ib}(\omega) = \varepsilon_{ib1}(\omega) + i\varepsilon_{ib2}(\omega)$ is the contribution of the interband transitions (bound electrons) to the dielectric permittivity of a metal, and $\varepsilon_D(\omega)$ is

the contribution of the free electrons, given by Drude theory as

$$\varepsilon_{\mathrm{D}}(\omega) = 1 - \frac{\omega_p^2}{\omega^2 + i\gamma\omega}. \tag{3}$$

Here,

$$\omega_p = \sqrt{\frac{4\pi n e^2}{m^*}} \tag{4}$$

is the bulk plasmon frequency, where n is the concentration of free electrons, e is the electron charge, m^* is the effective mass of a free electron, and, in the following equations, γ is the damping constant of plasma oscillations. In the approximation of small damping ($\varepsilon_2 \ll |\varepsilon_1 + 2\varepsilon_m|$), which is appropriate for noble metals, the condition of excitation of the SPR in NPs much smaller than light wavelength is the following [18]:

$$\varepsilon_1(\omega) = -2\varepsilon_m. \tag{5}$$

The SPR energy is then attained by substituting the complex dielectric permittivity for metal NPs from Eqs. (2) and (3) into Eq. (5):

$$\omega_{sp} = \sqrt{\frac{\omega_p^2}{1 + 2\varepsilon_m + \varepsilon_{\mathrm{ib1}}} - \gamma^2}, \tag{6}$$

where $\varepsilon_{\mathrm{ib1}}$ is the real part of the contribution of interband transitions to the permittivity of NPs. The plasmon damping constant can be expressed [18,19] as

$$\gamma = \gamma_\infty + A\frac{v_{\mathrm{F}}}{R}, \tag{7}$$

where R is the radius of the NP, γ_∞ is the size-independent damping constant caused by the scattering of free electrons on electrons, phonons, and lattice defects, A is a theory-dependent parameter that includes details of the scattering process (isotropic or diffuse scattering [18,43,44]), and v_{F} is the Fermi velocity in a bulk metal. We should note that a more precise theory exists on the size dependence of the surface plasmon damping constant $\gamma(R)$ [45]. This theory predicts the oscillating character of the dependence $\gamma(R)$ that results from the quasidiscrete spectrum of phonons in the NP. Electron scattering on long-wave phonons dominates in a metal and for metal NPs, the long-wave spectrum is limited by the size of the particle, which leads to oscillations in the

$\gamma(R)$ dependence. However, noticeable oscillations in the dependence $\gamma(R)$ appear for NPs smaller than approximately 15 nm. For larger particles, the oscillations are small and decrease as the particles increase in size. As a result, for larger particles, the dependence $\gamma(R)$ is nearly monotonically decreasing and thus is described well by expression (7). Since the NPs studied in our work are larger than 15 nm, our choice of the simplified expression (7) to describe the size dependence of the surface plasmon damping constant is appropriate. Since the NPs in the studied samples are not of monosize, their size distribution leads to a blurring of the slight oscillations of the damping constant for large NPs.

Considering the above, we may now analyze the influence of the temperature on the energy and width of SPR in metal NPs embedded in a host matrix. The first mechanism listed of the dependence of SPR on the temperature is the electron-phonon scattering within the metal NP. The size-independent damping constant γ_∞ depends on the temperature due to the temperature dependence of the electron-phonon scattering rate. With an increase in the temperature, the phonon populations in the metal increase leading to an increase in the probability of the electron-phonon scattering. This results in the increased scattering rate for the electrons. The γ_∞ dependence caused by the electron-phonon scattering is given by [46]

$$\gamma_\infty(T) = S\left[\frac{2}{5} + 3\left(\frac{T}{\Theta}\right)^5 \int\limits_0^{\Theta/T} \frac{x^4 dx}{e^x - 1}\right], \tag{8}$$

where Θ is the metal Debye temperature, and S is a constant [46]. Knowing the bulk damping constant γ_∞ for a certain temperature, such as room temperature, where $T_0 = 20\ ^\circ\mathrm{C}$, S can be calculated as

$$S = \frac{\gamma_\infty(T_0)}{\frac{2}{5} + 4\left(\frac{T_0}{\Theta}\right)^5 \int\limits_0^{\Theta/T_0} \frac{x^4 dx}{e^x - 1}}. \tag{9}$$

Thus, an increase in the electron-phonon scattering rate with the heating would also lead to an increase of the damping constant γ_∞. This would lead to the broadening of the SPR, as well as to its red shift in accordance with Eq. (6).

The second mechanism of the dependence $\varepsilon(T)$ is the thermal expansion of the NPs. With an increase

in the temperature, the volume of NP increases as

$$V(T) = V_0 (1 + \beta \Delta T), \tag{10}$$

where $\Delta T = T - T_0$ is the change in the temperature from room temperature $T_0 = 20$ °C, β is the volume thermal expansion coefficient, V_0 is the volume of NPs at $T_0 = 20$ °C. The density of free electrons in a metal particle is given by $n = N/V$, where N is the number of electrons, and V is the volume of the particle. Let us denote the free electron density at room temperature by n_0. Since the total number of free electrons in the NP is temperature-independent [47], given $N = n_0 V_0 = n(T) V(T)$ and by combining Eqs. (4) and (10), we obtain the bulk plasmon frequency

$$\omega_p = \sqrt{\frac{4\pi n_0 e^2}{m^* (1 + \beta \Delta T)}}. \tag{11}$$

Substituting Eq. (10) into Eq. (6), we obtain the expression for the frequency of the SPR in the metal NP

$$\omega_{sp} = \sqrt{\frac{\omega_{p0}^2}{(1 + 2\varepsilon_m + \varepsilon_{ib1})(1 + \beta \Delta T)} - \gamma^2}, \tag{12}$$

where $\omega_{p0} = \sqrt{4\pi n_0 e^2 / m^*}$ is the bulk plasmon frequency at room temperature. The thermal expansion of the NP would lead to a decrease in the concentration of free electrons in NPs and to a decrease in the energy of the SPR or to its red shift with increasing temperature. The damping constant of plasma oscillations depends on the size of the NP as $\gamma(R) \propto 1/R$ (see Eq. (7)). This is due to the scattering of free electrons on the surface of the NP. At the thermal expansion, the radius of the NP increases as

$$R(T) = R_0 (1 + \beta \Delta T)^{1/3}, \tag{13}$$

where R_0 is NP's radius at room temperature. Therefore, the NP thermal expansion would affect the frequency of SPR not only through the frequency of a bulk plasmon, but also by the size-dependent part of the plasmon damping constant. The volume expansion coefficient depends on the temperature according to [48] as

$$\beta(T) = \frac{192\rho k_B}{r_0 \phi (16\rho - 7Tk_B)^2}, \tag{14}$$

where k_B is the Boltzmann constant, and ρ, ϕ, r_0 are the parameters of the Morse potential $U(r) = \rho \left[e^{-2\phi(r-r_0)} - 2e^{-\phi(r-r_0)} \right]$ used in Ref. [48] to describe the interatomic interaction potential in Au. The linear and volume expansion coefficients are related through $\alpha = \beta/3$.

Having considered the thermal expansion of the NP, if it is free, we must now account for the fact that the NPs in our experiments were embedded in a silica matrix. Considering that the volume thermal expansion coefficient for silica is much smaller (1.65×10^{-6} K^{-1} for fused silica) than the coefficient for noble metals (e.g. 4.17×10^{-5} K^{-1} for Au), it might seem as though the silica host matrix would block the expansion of the NP. However, our fabrication procedure for the Me/SiO$_2$ composite samples relied on the formation of metal NPs in silica at a temperature of 1200 °C, which is higher than the maximum temperature used in our optical measurements (915 °C). Thus, the sizes of the NP and the hosting cavity of a silica matrix are equal only at the highest temperature, or 1200 °C. After the annealing at 1200 °C, the samples were cooled to room temperature. Upon cooling, both the NP and hosting cavity contracted. However, due to the considerable difference in the coefficients of thermal expansion, the metal NP contracted considerably stronger than the hosting cavity did. So, at any temperature lower than 1200 °C, the metal NP size is smaller than that of the hosting cavity of the silica matrix. In our experiments, we can therefore conclude that the metal NPs expanded freely, and that the matrix did not affect the thermal expansion of the NPs.

The third and final mechanism of temperature dependence of the SPR is the temperature dependence of the dielectric permittivity of the host matrix $\varepsilon_m(T)$. The reference data [49] show that the permittivity of silica increases with the temperature. From Eq. (12), we see that a temperature-induced increase in ε_m would lead to the red shift of the SPR as well. Summarizing the above arguments, we obtain the following expressions explaining the temperature dependences of the energy and width of the SPR in Au NPs in the silica host matrix:

$$\omega_{sp}(T) =$$

$$= \sqrt{\frac{\omega_{p0}^2}{(1 + \varepsilon_{ib1} + 2\varepsilon_m(T))(1 + \beta(T)\Delta T)} - \gamma^2(T)}, \tag{15}$$
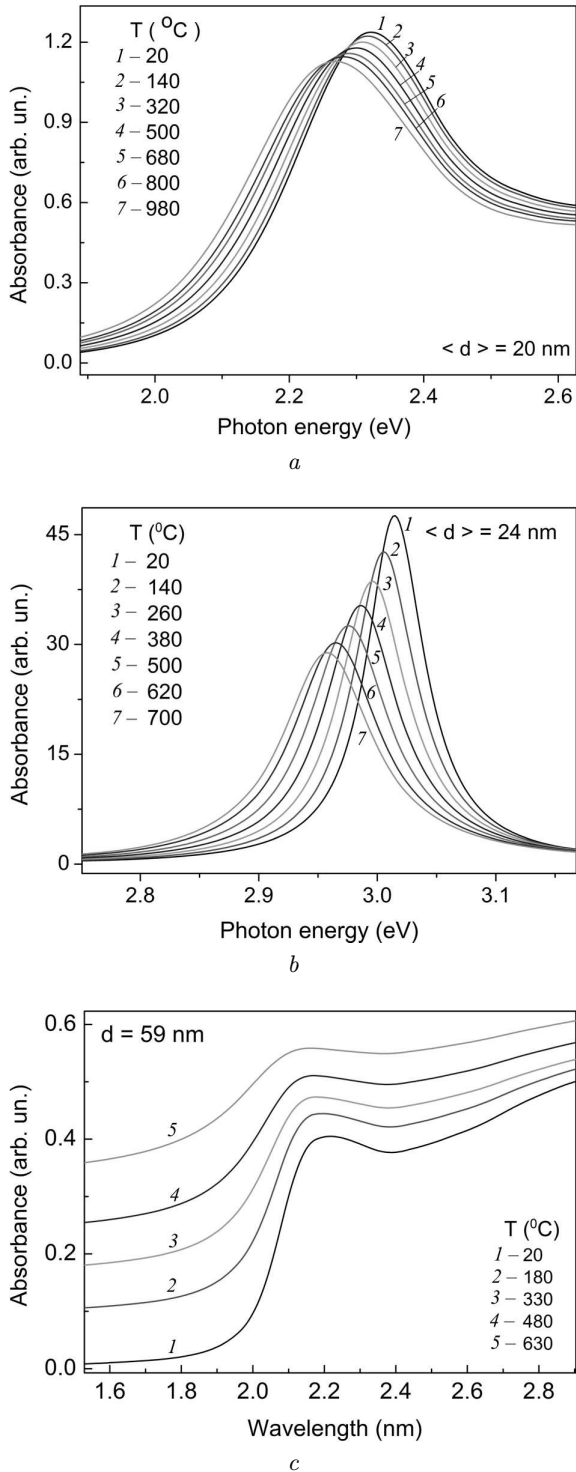
Fig. 8. Evolution of the calculated absorption spectrum of gold (*a*), silver (*b*), and copper (*c*) nanoparticle in silica with increasing temperature. (Modified from Refs. [37–39])

$$\gamma(T) = \gamma_\infty(T) + A\frac{v_F}{R(T)}, \qquad (16)$$

where the dependences $\gamma_\infty(T)$, $R(T)$ and $\beta(T)$ are given by Eqs. (8), (13) and (14), respectively.

1.5. Comparison of Experiment and Theory: Discussion

Here, we leverage the previously outlined theory to rationalize the experimental temperature dependences of the SPR energy and bandwidth for Au, Ag, and Cu NPs in silica. The absorption spectra of noble metal NPs in silica at various temperatures were calculated using Eq. (1). The temperature dependence of the silica host matrix was taken from Ref. [49]. Considering the temperature dependence of the dielectric permittivity of NP, first, we calculated the contribution of interband transitions in of NP as

$$\varepsilon_{ib}(\omega) = \varepsilon_\infty(\omega) - \varepsilon_{D\infty}(\omega), \qquad (17)$$

where ε_∞ is the dielectric permittivity of a bulk metal taken from Ref. [50], $\varepsilon_{D\infty}(\omega)$ is the Drude term for a bulk metal (or the contribution of free electrons) calculated by Eq. (3). We used the values for ω_p and γ_∞ from Ref. [51]. We then calculated the temperature-dependent dielectric permittivity of the NP as follows

$$\varepsilon(\omega, T) = \varepsilon_{ib}(\omega) + \varepsilon_D(\omega, T), \qquad (18)$$

where $\varepsilon_D(\omega, T)$ was calculated using Eq. (3). In calculating $\varepsilon_D(\omega, T)$: (1) the temperature-dependent bulk plasmon frequency was calculated by $\omega_p(T) = \omega_{p0}/\sqrt{1 + \beta(T)\Delta T}$, where ω_{p0} was taken from Ref. [51] and $\beta(T)$ were calculated by Eq. (14); (2) the temperature-dependent damping constant $\gamma(T)$ was calculated by Eq. (16), where $\gamma_\infty(T)$ was calculated by Eqs. (8)–(9) and $R(T)$ by Eq. (13). Additionally, we used the values for the Fermi velocity in bulk metals from Ref. [51], the values for parameter A were estimated from the fitting of the experimental size dependence of the SPR bandwidth at $T_0 = 20\,°C$, and, finally, we used the parameters of the Morse potential ρ, ϕ, r_0 from Ref. [52].

The trend of the calculated absorption spectrum of Au, Ag, and Cu NPs in silica with increasing temperature is presented in Fig. 8, *a*, *b*, and *c*, respectively. Increasing the temperature led to a red shift and broadening of the SPR band for each metal. This trend similarly parallels the one observed experimentally. To quantitatively check our above assumptions

120

of the physical mechanisms of these temperature-induced phenomena, we also calculated the temperature dependences of the shift and broadening of SPR in noble metal NPs. To compare the respective experimental and calculated dependences correctly, we achieved the theoretical values of the SPR energy and bandwidth by peak-fitting the calculated spectra with Lorentzian peaks, since the same method was used to determine the corresponding experimental values. The realized calculated temperature dependences of the SPR energy and bandwidth are presented by solid lines in Figs. 3, 5, and 7 for Au, Ag, and Cu NPs, respectively. The corresponding experimental dependences are shown by points on these figures as well, and we observed a resultant agreement of the experimental and calculated dependences. This supports the correctness of our theoretical model. The only deviation observed between experiment and theory lies in the temperature dependence of the SPR bandwidth in Au NPs at temperatures higher than about 750 °C. It is likely that this deviation is due to the premelting or melting of Au NPs, which is accompanied by a jump of the SPR bandwidth. Such an effect was reported for Cu, Au, Ag, and Sn NPs in Refs. [41, 53–55].

As noted, the theoretically calculated dependences are due to the contributions of three mechanisms. Those mechanisms are the electron-phonon scattering within the NP, the thermal expansion, and the temperature dependence of the dielectric permittivity of a host matrix. To better understand the relative contribution of each mechanism to the total temperature effect, we performed calculations for the temperature dependence of the SPR energy and for the width. The findings are similar for all noble metals, which supports the similarity of the physical mechanisms of the observed temperature-induced SPR red shifts and broadenings in noble metal NPs. Thus, the results of calculations are presented in Fig. 9 only for Au NPs. From Fig. 9, *a*, one observes that the thermal expansion is the dominant mechanism of the temperature-induced red shift of SPR. Contributions of the increase of the electron-phonon scattering rate and the increase of the permittivity of a host matrix with the temperature are close to each other and are relatively small compared to the thermal expansion. The dominant mechanism of the temperature-induced broadening of SPR is the electron-phonon scattering seen in Fig. 9, *b*. Thermal expansion of the
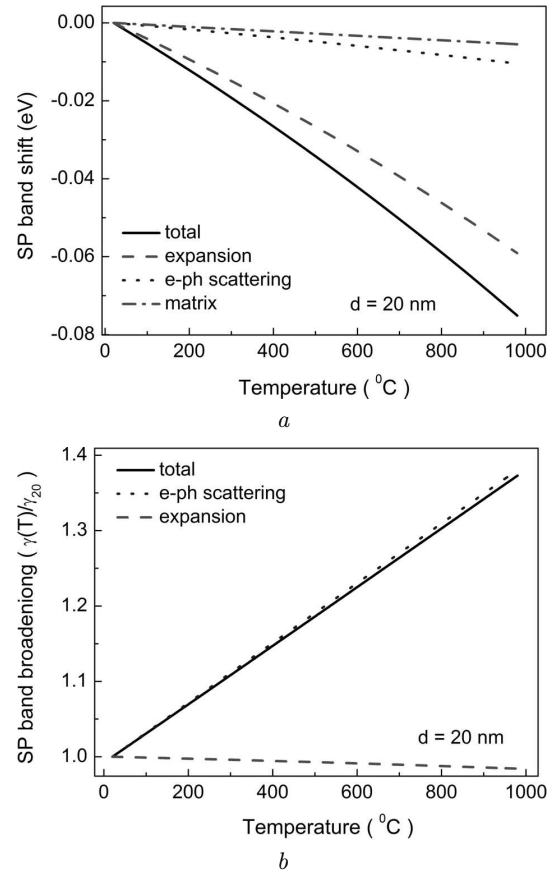

Fig. 9. Calculation of the contributions of different mechanisms to the temperature-induced (*a*) shift and (*b*) broadening of SPR in a 20-nm gold NP in silica. Solid lines mark the total shift or broadening, dashed lines – contribution of the thermal expansion of the NP, dotted lines – the electron-phonon scattering in the NP, dash-dotted lines – the temperature dependence of the dielectric permittivity of a host matrix. (Modified from Ref. [37])

NP leads to a very small decrease in the SPR width. However, this decrease is negligible and can be neglected. Temperature dependence of the permittivity of a host matrix does not affect the width of the SPR. Thus, the thermal expansion of the NP produces the red shift, and the electron-phonon scattering produces the broadening of SPR with an increase in the temperature. From Figs. 3, 5, and 7, *a*, we see that the red shift rate of the SPR with increasing temperature is the same for all noble metal NPs and for all studied sizes. This indicates that the volume thermal expansion coefficient is size-independent for noble metals in the studied range of NP sizes. Concer-

ning the temperature dependences of the SPR width and the damping constant $\gamma(T)$, one observes from Figs. 3, 5, and 7, *b* that both experimental and theoretical dependences are nearly linear. This observation agrees entirely with the well-known fact that the rate of electron-phonon scattering increases linearly as the temperature increases, when the temperature considerably exceeds the Debye temperature, $T \gg \Theta$, from Eq. (8).

1.6. Conclusions

The temperature dependences of the energy and width of SPR in noble metal (Au, Ag, Cu) NPs with a mean size in the range from 17 to 60 nm, which were embedded in a silica glass host matrix, were studied in a broad temperature range from 17 to 915 °C. As the temperature increased, a red shift and broadening of the SPR occurred. The theoretical models including the phenomena of the electron-phonon scattering in the NP, the thermal expansion of the NP, and the temperature dependence of the dielectric permittivity of the host matrix were studied and concur with the observed temperature behavior of SPR in Au NPs. As the temperature of the particle increases, the volume of the NP increases and the density of free electrons decreases. The lower electron density leads to a lower plasma frequency of the electrons and subsequently to the red shift of the SPR. The rate of electron-phonon scattering increases with the heating. This leads to the increase of the damping constant of plasma oscillations and, as a result, to the red shift of the SPR. The dielectric permittivity of silica increases with the temperature, also leading to the red shift of the SPR. The numerical calculations of the temperature dependences of the SPR energy and width agree strongly with the respective experimental data and reinforce the validity of the chosen theoretical models. Thermal expansion of the Au NPs turned out to be the dominant mechanism of the temperature-induced red shift of SPR in metal NPs. However, the dominant mechanism of the broadening of SPR occurring with an increase in the temperature is the electron-phonon scattering in the NP.

2. Temperature Dependence of Photoluminescence from Metal NPs

2.1. Introduction

Photoluminescence (PL) of metals is a rare phenomenon, and the previous experiments [57] have resulted in a quantum yield of noble metal PL in the range of about 10^{-10}, quite a low yield. This is primarily because metals do not possess an energy gap between occupied and unoccupied states of electrons within the conduction band. The excited electron can then recombine non-radiatively with the hole, leading to a very low probability of radiative transitions and luminescence processes [58–60]. The PL of bulk Ag [61], Au, and Cu [57] was experimentally observed near the edge of interband absorption in these metals. The PL probably stems from the direct interband radiative recombination of *sp*-electrons of the conduction band with holes in the valence *d*-band states with momentum smaller than the Fermi momentum. However, PL from metal NPs (NPs) has not been studied thoroughly, partly due to the low probability of corresponding radiative transitions in the metals noted above. The PL of noble metal NPs has been reported for Ag [62–65], Au [66, 67], and Cu [68, 69]. Each of these studies revealed a maximum of the PL band close to the interband absorption edge, so the PL was attributed to the interband radiative transitions.

The huge enhancement (up to 8 orders of magnitude) of the PL quantum yield for small noble metal NPs was recently observed [62, 66–69]. The nature of this large enhancement is the excitation of the SPR in the NP. Excitation of the SPR leads to the formation of an enhanced local electric field close to the surface of the particle (both inside and outside) [18–21], and such a strong local electric field sufficiently enhances the induced radiative interband transitions in the metal NPs, subsequently leading to a significant enhancement of their PL. A theory of surface plasmon induced enhancement of PL from metal NPs was developed by Boyd *et al.* [70]. The effect of this enhancement is very important, because it provides an opportunity to use such NPs for practical applications in the cell bioimaging. Metal NPs for the bioimaging have several advantages over organic fluorophores (fluorescent proteins and organic dyes) and semiconductor quantum dots, such as the photostability and biocompatibility, with less blinking. While the size dependence of PL from metal NPs is straightforward (scattering of free electrons on the surface of NP and the radiation damping of surface plasmons) [62], the temperature dependence of the NP PL has not been examined closely.

In our recent work [65], we studied the temperature dependence of PL of Ag NPs in the range of 78

to 298 K. We observed an appreciable decrease in the PL quantum yield as the temperature increased. We hypothesized that this effect resulted from an increase in the plasmon damping with the temperature, due to an increase in the electron-phonon scattering rate, highlighted in the previous section. In our recent work [68], we reported the results of studying the temperature influence on the PL spectra of spherical Cu NPs with a size of 17 nm, embedded in a silica host medium in the temperature range from 78 to 298 K. The intensity of PL spectra increases consistently with the temperature, opposite to that of Ag NPs. Anomalous temperature dependence for Cu NPs plays a key role in the interband transitions in Cu. Hubentahl showed [71] that the interband transitions are a significant additional mechanism of SPR damping, when the SPR frequency is close to the onset of interband transitions. Such a mechanism is not important for Ag NPs due to the spectral separation of the SPR and interband transitions and is very significant for Cu NPs, where SPR is very close (slightly higher by energy) to the onset of interband transitions. We found both experimentally and theoretically that a temperature-induced red shift of SPR in Cu NPs leads to a decrease of interband transitions caused by the SPR damping and to a better overlapping of the SPR and PL bands of Cu. These two mechanisms lead to an increase in the electron-phonon scattering rate as temperature increases, subsequently causing an anomalous increase in the quantum yield of PL.

2.2. Experiment

Fabrication procedures of Ag and Cu NPs in a silica host matrix were carried out according to the known experimental procedure described in subsection 1.2. PL spectra of the Ag/SiO_2 and Cu/SiO_2 nanocomposites were measured using a Cary Eclipse (Varian Inc.) fluorescence spectrophotometer. The PL of Ag and of Cu NPs was excited by a single monochromatic line with wavelengths of 310 nm and 355 nm, respectively (spectral half-width of 5 nm), cut from the continuous emission spectrum of a pulse Xe lamp. In our experiment, the repetition rate of the pulses was 80 Hz, the pulse duration was 2 μsec, and the pulse power density was 1.3×10^3 W/cm^2. While the measurements were collected, the samples were placed in a nitrogen bath cryostat Optistat DN (Oxford instruments). The PL spectra were measured at
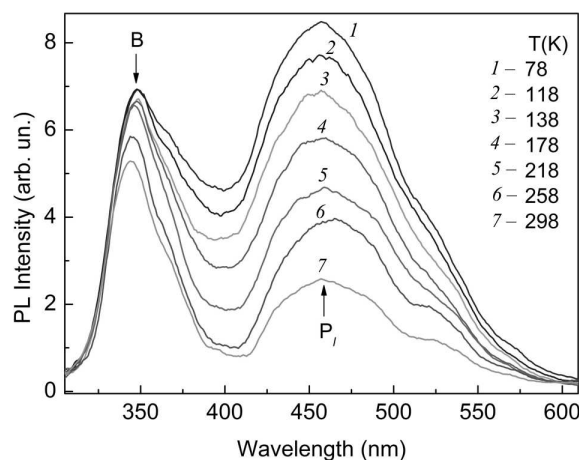

Fig. 10. Evolution of the PL spectrum of Ag NPs with a mean size of 17 nm in silica with increase in the temperature from 78 to 298 K. The presented spectra were obtained by the subtraction of the spectra of a pure silica matrix from the total spectra of the Ag/SiO_2 composite. Excitation wavelength is 310 nm. (Modified from Ref. [65])

various temperatures ranging from 78 to 298 K. The temperature was maintained and measured with the use of an Intelligent Temperature Controller ITC503S (Oxford instruments), and each spectrum was measured at its respective stabilized temperature.

2.3. Temperature Dependence of Photoluminescence from Metal NPs: Experimental Results

2.3.1. Ag NPs

We measured the PL spectra of several Ag/SiO_2 composites containing Ag NPs of differing average sizes (from 8 to 30 nm) at various temperatures ranging from 78 to 293 K [65]. Additionally, the PL of an annealed silica sample prepared from xerogel without the Ag dopant ($AgNO_3$) was measured in the same temperature range. To separate the PL spectrum of the Ag NPs from the spectrum of the silica host at a certain temperature, the latter was subtracted from the original spectrum of the composite. Figure 10 shows the temperature behavior of the PL spectra of Ag NPs with an average size of 17 nm, as the temperature increased from 78 to 298 K. The results show that an increase in the temperature leads to a considerable decrease in the total PL intensity, indicating a strong temperature dependence of the PL quantum yield in Ag NPs. One observes
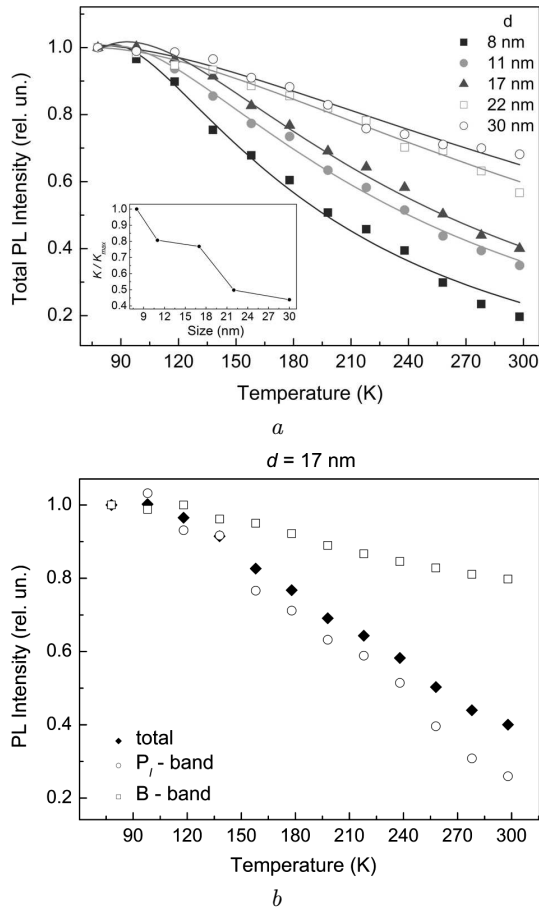
Fig. 11. Experimental temperature dependences of the normalized total intensity of PL from Ag NPs of various sizes in silica. The experimental points are fitted by expression (20). Inset shows the size dependence of the normalized strength of the electron-phonon coupling in Ag NPs (a). Experimental temperature dependences of the normalized intensities of the B and P_l bands and the total intensity for Ag NPs with an average size of 17 nm (b). (Modified from Ref. [65])

that the PL quantum yield decreases, as temperature increases. Figure 11, a presents the experimental temperature dependences of the total intensity of the PL spectra from Ag NPs of various sizes. The decrease in the PL quantum yield with an increase in temperature is typical of Ag NPs of all sizes in the studied interval from 8 to 30 nm. Additionally, the temperature-induced decrease of the PL quantum yield becomes stronger, as the size of the NP decreases. The origin of this effect lies in the size dependence of the electron-phonon coupling strength, which is discussed below in subsection 2.5.

From Fig. 10, one can see that the observed PL spectra consist of two bands, as reported in our recent work [6], where the size dependence of the PL from Ag NPs was studied. These bands have been denoted as P_l and B. Both bands have been rationalized in Ref. [6] as originating from the PL of Ag NPs enhanced by a strong local electric field of surface plasmons excited within the NPs. The maximum of the high-energy B band is found at approximately 345 nm, which is very close to the maximum (3.75 eV or 330 nm) of the PL band for bulk Ag [60, 72]. Such a PL band was experimentally observed for the first time in bulk Ag in Ref. [72] and was attributed to the direct radiative interband recombination of the conduction band electrons with holes in the valence band that had been scattered to momentum states, which were less than the Fermi momentum [60]. It is also important to note that the maximum of the B band is close to the interband absorption edge of bulk Ag (3.2 eV or 388 nm) [60]. Similarly, PL bands with maxima around 330 nm were observed for Ag NPs in Refs. [63, 73]. Therefore, we attribute the B band in our PL spectra to the interband radiative transitions in Ag NPs. The red shift of the B band relative to the PL band from bulk Ag is caused by the coupling of the incoming (excited) and outgoing (emitted) photons with the SPR as discussed below. The second PL band, denoted as Pl, was observed at wavelengths close to the SPR. This band originates from the low-energy wing of the interband B and is strongly enhanced by the local field of the surface plasmons, since the local field enhancement factor reaches a maximum at the resonant frequency of the SPR and decreases rapidly with the detuning from the SPR [74]. PL bands from Ag NPs and nanorods located near the SPR were observed experimentally and reported in the literature [6, 63, 64, 75]. Figure 10 shows that, although the intensities of both the B and P_l bands decrease, as the temperature increases, the decrease is considerably stronger for the low-energy P_l band. This is also clearly seen in Fig. 11, b, where the temperature dependence of the intensity is shown separately for each band. This is in accordance with the existing knowledge, since the low-energy P_l band is spectrally located nearer to the SPR, so is much more sensitive to changes in the plasmonic enhancement factor than the high-energy B band would be; the B band overlaps with the SPR only slightly.

2.3.2. Cu NPs

The PL spectra of Cu/SiO$_2$ composite glasses with 17-nm Cu NPs were studied at varying temperatures ranging from 78 to 298 K [68]. The PL spectra for the pure silica sample (without Cu NPs) were also measured in the same temperature interval, so that just as with Ag NPs, we could separate the PL spectrum of the Cu NPs from the spectrum of the silica host at a certain temperature by subtracting the pure samples from the original spectrum of the Cu/SiO$_2$ composite. Figure 12 presents the trend of the PL spectra of Cu NPs with a mean size of 17 nm, as the temperature increased.

The intensity of the silica PL spectrum is quite low compared to that of Cu NPs, so the contribution of silica to the total spectrum of Cu/SiO$_2$ composite can be neglected. Figure 12 shows that the measured PL spectrum of Cu NPs has a single asymmetric band with a low-energy tail with maximum at approximately 620 nm. This aligns with other observations of PL from Cu NPs [69]. This spectral position is very close to that of the PL band of bulk Cu (2.1 eV or 595 nm) [57,60]. It is important to note that the maxima of PL bands of both bulk Cu and of Cu NPs coincide with the onset of interband transitions in bulk Cu (2.0 eV or 620 nm) [50]. The nature of the observed spectra may stem from the inherent PL of Cu NPs or copper-silica interface complexes. Such complexes may be formed due to the chemical bonding between the Cu atoms of the NP surface and atoms of the matrix. The possibility of such complex formation was described in Refs. [76–78]. However, as illustrated in Ref. [78], the PL bands of the Cu–SiO$_2$ interface complexes exist at energies of 3.1 eV (400 nm) and higher. The intensity of the PL band with a maximum at about 600 nm [78] increased considerably at the high-temperature annealing of the composite Cu/SiO$_2$ under conditions like those in our experiment; this is due to the reduction of metallic Cu and the formation of Cu NPs. The 600-nm band was attributed in Ref. [78] to the intrinsic PL from the Cu NPs. A similar asymmetric band at 620 nm with low-energy tail was observed for Cu NPs in a colloidal solution [69]. Based on this evidence, it is reasonable to conclude that the tail does not originate from the PL of Cu–SiO$_2$ interface complexes. Thus, the band with a maximum at about 620 nm observed for our samples is likely due to inherent PL from Cu NPs. We can also attribute the PL observed in our
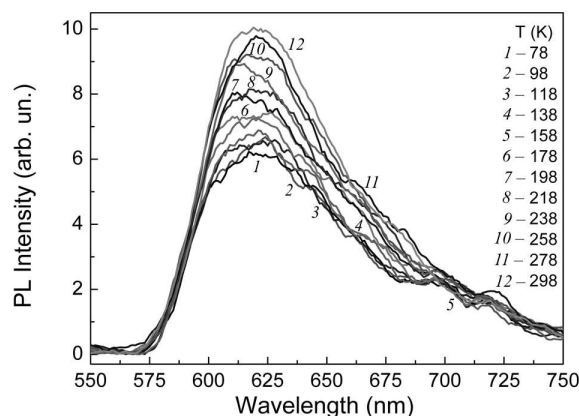

Fig. 12. Evolution of the PL spectrum of Cu NPs with increase in the temperature from 78 to 298 K. Excitation wavelength is 355 nm. (Modified from Ref. [68])

experiments to the direct radiative interband recombination of the conduction band electrons with holes in the valence band in Cu NPs. Our estimation of the quantum yield of observed PL is about 10^{-5}, which is significantly higher than the quantum yield for bulk Cu at 10^{-10}, Ref. [57]. As noted above, it is well-established knowledge that the strong local electric field of surface plasmons excited in the NPs causes such a large enhancement of the PL of metal NPs.

Let us turn to analyzing the temperature dependence of the Cu NPs PL spectrum shown in Fig. 12. Instead of the expected decrease in the PL intensity with increasing temperature, we observed an appreciable increase (multiplied 1.5 times) in the PL intensity, indicating a strong anomalous temperature dependence of the PL quantum yield for Cu NPs. This is a strange anomalous dependence, opposite to the observation of the PL intensity decreasing with the temperature that is often observed for many materials including semiconductors and metals. Indeed, as previously noted, an apparent decrease in the PL quantum yield for Ag NPs is observed with increasing temperature. Figure 13 presents the attained experimental temperature dependence of the total intensity of the PL band of Cu NPs with mean size of 17 nm, while the silica PL intensity decreases, as temperature increases, which is the opposite behavior compared to that of Cu NPs. Therefore, we suggest that the observed increase in the PL intensity from Cu/SiO$_2$ composites is not related to the silica matrix. This indicates that such anomalous temperature behavior is an inherent property of Cu NPs. What is the origin
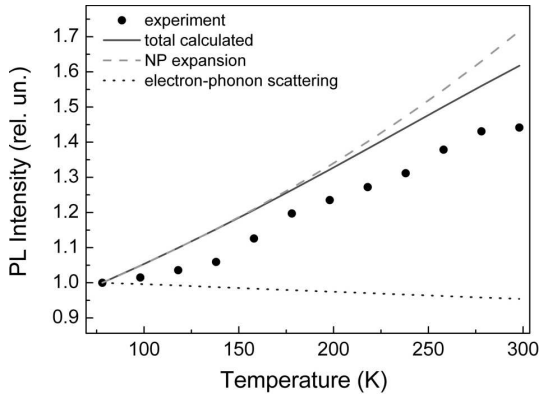
Fig. 13. Temperature dependence of the intensity of PL from copper NPs 17 nm in size. Dots – experimental dependence, lines – calculated ones. Red line – calculated dependence obtained with considering both NPs thermal expansion and electron-phonon scattering rate ($\gamma_{\mathrm{e-ph}}$) increase with temperature; green dashed line – contribution of the thermal expansion of NPs causing the SPR red shift; blue dotted one – contribution of the electron-phonon scattering. All the dependences are normalized to the values at $T = 78$ K. (Modified from Ref. [68])

of such an anomalous temperature dependence of PL intensity for Cu NPs? Below, we explain that both spectral proximity of the SPR and the onset of the interband transition in Cu NPs play key roles in such dependence.

2.4. Temperature Dependence of Photoluminescence from Metal NPs: Theoretical model

G.T. Boyd *et al.* developed a theory of surface plasmon enhancement of PL from nano-sized metals [70]. This enhancement is due to the strong local electric field near the metal NP, where surface plasmons are excited. As previously noted, the electric fields of incoming (excited) and outgoing (emitted) photons are enhanced via the coupling to the SPR. This significant plasmonic enhancement allows a reliable observation of the PL from metal NPs. Here, we analyze the influence of the temperature on the plasmonic enhancement factor and, subsequently, on the PL quantum yield. According to Boyd's theory, the local electric field inside a NP is enhanced by a factor known as the local field correction factor

$$L\left(\omega,T\right) =$$
$$= \frac{D^{-1}}{\frac{\varepsilon(\omega,T)}{\varepsilon_m(T)}-1+D^{-1}\left[1+i\frac{4\pi^2 V(T)(1-\varepsilon(\omega,T))\varepsilon_m^{1/2}(T)}{3\lambda^3}\right]}, (19)$$

where D is the depolarization factor ($D = 1/3$ for spherical particles), $\varepsilon(\omega,T)$ is the complex dielectric permittivity of the metal, $\varepsilon_m(T)$ is the dielectric permittivity of the host matrix, λ is the light wavelength, $V(T) = \pi d^3(T)/6$ is the NP volume, and $d(T)$ is its size (diameter). The power of the single-photon luminescence $P(\omega_l, T)$ from a metal NP excited by a photon with the energy $\hbar\omega_{\mathrm{exc}}$ is given by

$$P(\omega_l, T) = 2^4 \beta(\omega_l)|E_0|^2 V|L^2(\omega_{\mathrm{exc}}, T)L^2(\omega_l, T)|, (20)$$

where E_0 is the electric field of the incident (exciting) light, and $\beta(\omega_l)$ is a function describing the PL spectrum of a bulk metal. The PL spectrum of metal NPs may be calculated using the local enhancement factors for excited $L(\omega_{\mathrm{exc}}, T)$ and emitted $L(\omega_l, T)$ photons.

The temperature dependence of PL of metal NPs appears through the temperature dependence of these local enhancement factors. Namely, L depends on T due to the temperature dependence of the dielectric permittivity of the NP (ε), along with the NP's volume V and the permittivity of the host matrix ε_m. Concerning the dependence $\varepsilon_m(T)$, as previously discussed [37], this dependence is very small and only affects the SPR frequency and the damping constant very slightly. Therefore, we neglect the dependence $\varepsilon_m(T)$ and consider ε_m to be a constant. The temperature-dependent dielectric permittivity of a metal NP may be calculated by the expressions described in subsection 1.4.

2.5. Comparative Analysis and Discussion of the Temperature Dependence of Photoluminescence of Ag and Cu NPs

Based on the above theoretical model, we calculated the PL spectra of Ag and Cu NPs with a size of 17 nm in the silica host matrix at temperatures ranging from 78 to 298 K. The results of these calculations are shown in Fig. 14. An increase in the temperature leads to a decrease in the PL intensity for Ag NPs, as seen in Fig. 14, *a*. As noted, an opposing dependence was observed for Cu NPs, since an increase in the temperature leads to an increase in the PL intensity shown in Fig. 14, *b*. Such results are in full agreement with the experimental behavior of PL at the varying temperature for NPs of both metals. Moreover, there is a quantitative agreement

between experiment and theoretical calculations performed. This is seen in Fig. 11, *a* for Ag NPs and in Fig. 13 for Cu NPs. Next, we consider the physical causes for such different temperature dependences of the intensity of PL from Ag and Cu NPs.

Considering subsections 1.4 and 2.4, the temperature can influence the PL from the metal NPs due to (1) electron-phonon scattering, and (2) thermal expansion of the NP with increasing temperature. The rise of the rate of electron-phonon scattering with increasing temperature (see Eq. (8) would lead to an increase in the SPR damping constant with a corresponding decrease in the plasmonic local field enhancement factor from Eq. (19). This would lead to a decrease in the PL intensity, as the temperature increases. Indeed, the respective decrease of the quantum yield of PL from Ag NPs is observed. As noted in Section 1, the electron-phonon scattering very nearly does not even affect the frequency of the SPR. In turn, the temperature-induced volume expansion of the NP affects the SPR frequency, causing a red shift, as the temperature increases, and barely affects the plasmon damping constant (SPR width). Thus, in Ag NPs, where the SPR and the interband transitions are spectrally separated, the temperature-induced red shift of the SPR does not affect the quantum PL yield. So, the decrease in the quantum yield of PL from Ag NPs with increasing temperature is caused by an increase in the rate of electron-phonon scattering.

A completely contrasting situation occurs for Cu. For Cu NPs in silica, the onset of interband transitions (at approximately 650 nm) occurs at a lower-energy than the SPR (560–590 nm). At wavelengths shorter than 650 nm, an increase in the imaginary part of the dielectric permittivity of Cu, ε_2, occurs reflecting an increase in the contribution of the interband transitions, see Fig. 15. A considerable spectral overlap of the SPR and interband transitions takes place. Therefore, the red shift of the SPR occurring due to NP expansion would increase the overlap of the SPR and the interband-related PL in Cu NPs, Fig. 15. This effect would lead to an increase in the plasmonic field enhancement factor and would lead to an increase in the PL quantum yield. An additional mechanism of the temperature dependence of PL from Cu NPs exists. Hubentahl recently showed [71] that interband transitions are a significant additional mechanism of SPR damping, when the SPR
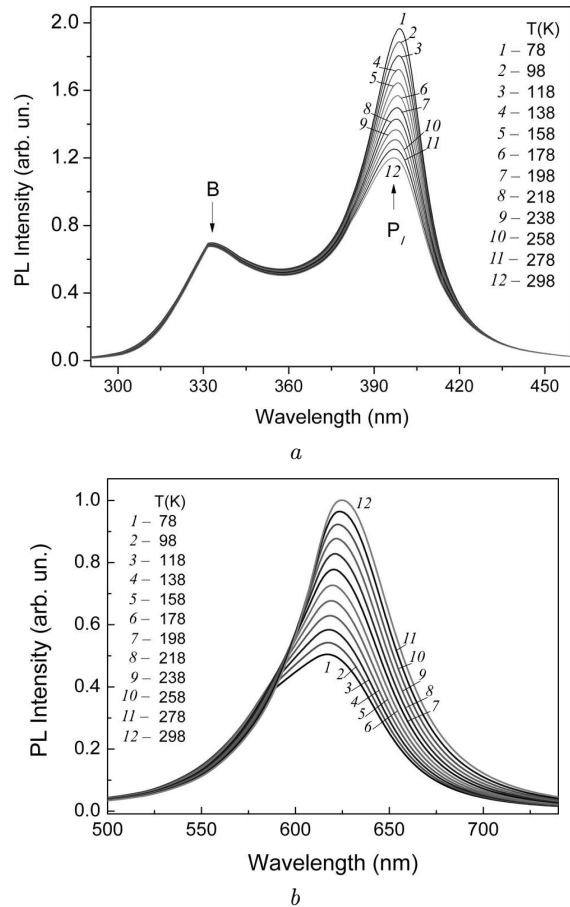

Fig. 14. Calculated evolution of the PL spectrum for silver (*a*) and copper NPs 17 nm in size in silica with increase in the temperature from 78 to 298 K. (Modified from Refs. [65] and [68])

frequency is close to the onset of interband transitions. At photon energies higher than the onset of interband transitions, the energy of a plasmon can be transferred to a single electron, which creates an interband transition, as previously suggested by D. Dalacu *et al.* [79]. Such a plasmon damping process differs from the Landau damping, which is due to intraband transitions. For photon energies well below the onset of the interband transition, the plasmon energy is too low to permit an interband transition, and such a mechanism of plasmon damping is not crucial. The red shift of the SPR with increasing temperature leads to a decrease in the contribution of interband transitions to the plasmon damping constant at the frequency of the SPR, see Fig. 15. Such a decrease in the SPR damping would lead to an in-
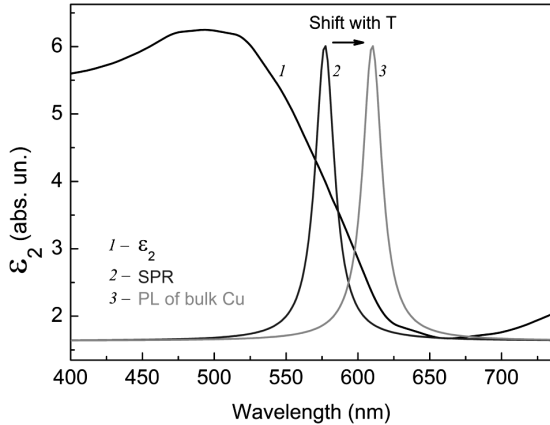
Fig. 15. Illustration of the physical principles causing the increase in the PL intensity from copper NPs occurring due to a red shift of SPR with increasing temperature. ε_2 is the imaginary part of the dielectric permittivity of copper. The SPR in Cu and PL band of bulk Cu are schematically marked by red and green lines, respectively. (Modified from Ref. [68])

crease in the plasmon field enhancement factor and, correspondingly, to an increase in the PL intensity.

As noted, two distinct physical mechanisms cause the temperature dependence of the quantum yield of PL from Cu NPs. The electron-phonon scattering decreases the PL quantum yield. By contrast, the thermal expansion of the NPs leads to the SPR red shift. The red shift then leads both to an increase in the overlap of the SPR and PL band and to the interband transition-related decrease in the plasmon damping that causes an increase in the PL quantum yield with increasing temperature. To assess the contributions of each mechanism to the total temperature dependence of the PL intensity, we performed additional calculations. To determine the contribution of the aforementioned processes related to the thermal expansion of the NP, we considered the rate of electron-phonon scattering to be temperature-independent, performing calculations for the value at 78 K, where $\gamma_{e-ph} = \text{const} = \gamma_{e-ph,78}$. The respective dependence of the PL intensity is shown in Fig. 13 by a dashed green line. As expected, the NP thermal expansion leads to an increase in the PL intensity with increasing temperature. To determine the contribution of the electron-phonon scattering, we excluded the thermal expansion by taking the volume expansion coefficient as $\beta = 0$. The corresponding calculated temperature dependence of the PL intensity is presented in Fig. 13 by a dotted blue line. As ex-

pected, the electron-phonon scattering leads to a decrease in the PL intensity. Thus, Fig. 13 shows that the contribution of the NP thermal expansion is much larger than that of the electron-phonon scattering to increasing the PL intensity, as the temperature increases. A key factor in the observed anomalous temperature dependence of the PL intensity is the interband transitions, which contribute significantly to the nature of the dielectric permittivity of Cu NP at the SPR frequency.

The phenomenon of the temperature dependence of the quantum yield of PL from metal NPs should occur for other metals. Our theoretical model can describe this phenomenon in other metal NP systems. It should be noted that the sign of the effect and its magnitude depends (1) on the magnitude of the plasmonic enhancement of the local field and (2) on the relative spectral location of the SPR and the PL band of a metal. This phenomenon would manifest itself most strongly in "plasmonic" metals such as Ag, Au, and Cu, where the SPR damping is lowest; this would provide a sufficiently large enhancement of PL from the metal NP. It would be interesting to examine the effect of temperature dependence on the quantum yield of PL from an object external to the metal NP. Recently, we observed the strong temperature dependence of the intensity of PL from rhodamine 6G [80] and fullerene C_{60} [81], molecules which are located in the vicinity of Au NPs. This effect is due to the temperature dependence of the plasmonic local field correction factor in metal NPs described by a model similar to the one considered in the review.

2.6. Conclusions

We experimentally studied the temperature dependence of PL from spherical Ag and Cu NPs embedded in a silica host medium in a temperature interval from 78 to 298 K. The PL spectra of both Ag and Cu NPs were theoretically examined and found to be a result of radiative interband transitions enhanced by the coupling of excited and emitted photons to the surface plasmons excited in the NPs.

The quantum yield of PL from Ag NPs decreased, as the temperature increased. This temperature dependence was explained as a result of a decrease in the plasmonic enhancement factor occurring due to an increase in the electron-phonon scattering rate. The theoretical calculations of the temperature behavior

of Ag NP PL spectra agree with the results of the experimental observations, proving the above interpretation. We also observed that the temperature dependences of the PL quantum yield are stronger for smaller Ag NPs. This effect was caused by the dependence of the electron-phonon coupling strength on the NP size, as shown above. The strength of the electron-phonon coupling increases by 2.3 times, as the NP size decreases from 30 to 8 nm.

The quantum yield of PL from Cu NPs increased by almost 1.5 times, as the temperature increased from 78 K to 298 K. We discussed two physical mechanisms, which caused the temperature dependence of the PL quantum yield: the first of these was the electron-phonon scattering responsible for a decrease in the PL intensity with increasing temperature. The second mechanism is the red shift of SPR with increasing temperature, which increases the spectral overlap of the SPR with the PL band of Cu, as well as decreases the interband-transition related damping of plasmons. A theoretical model considering these two mechanisms was used to explain the observed temperature behavior of the PL spectrum of Cu NPs. The results of calculations agree with the experimentally observed results, proving the correct model was used. The calculations showed that the contribution of the red-shift-related processes to the temperature dependence of the PL intensity significantly exceeds the contribution of the electron-phonon scattering. Thus, the interplay between the SPR and the interband transitions plays the critical role in the observed anomalous dependence of the quantum yield of PL from Cu NPs.

3. Light-Induced Heating of Metal NPs: Dependence on Detuning from SPR

3.1. Introduction

In addition to the thermo-optical plasmonic effects considered above, another effect has captured the attention of many researchers. This is the heat generation by metal NPs under an optical illumination [82–84]. The NPs serve as highly efficient, localized heat sources at the nanometer-scale length. This unique property suggests numerous potential applications in areas such as solar energy [85, 85, 87, 88], chemical catalysis [89, 90], protein imaging [91, 92], and biomedicine [93, 94]. Heating of metal NPs im-

mersed in liquid results in a vapor generation under continuous-wave (CW) and pulsed laser excitations [85, 86, 95–100]. Heat can create changes in the optical characteristics of a surrounding medium (which provides the refractive index) that can be recorded optically. Another important phenomenon is a phase transformation in the surrounding material caused by the heating of metal NPs [85, 86, 98]. The physical nature of the SPR-mediated heating of metal NPs is the scattering of free electrons involved in plasma oscillations on phonons, electrons and, in defects of the crystal lattices. Such scattering causes a damping of plasma oscillations, leading to the heating of NPs with the subsequent transfer of heat to the surrounding medium. The heating effect should have a resonant character, or, in other words, the heating should become especially strong under the SPR conditions, when the frequency of incident photons is close to the SPR frequency of the metal NP. Since metal NPs have a very low light emission quantum yield, almost all of the absorbed light energy is converted to the heat energy. This heating effect can be strongly enhanced in the presence of several NPs [85, 86, 98] such as in dense ensembles of NPs. There are two mechanisms of such increase: in the heating one is an accumulative effect and another one is the plasmon coupling of NPs. Resultant heat depends on the inter-NP distance and on the NP arrangement or configuration.

It is very important to measure the temperature of the metal NPs at their plasmon heating. An attempted direct measurement of the metal NP temperature has been reported by H.H. Richardson *et al.* [98]. This measurement was achieved by measuring the power threshold for the melting of Au NPs embedded in ice. Richardson's work made it possible to determine the NP surface temperature. Another interesting approach used was a complex formed from both a semiconductor and metal NPs [92]. These NPs were linked to each other with a polymer; the length of the polymer chain was strongly temperature-dependent. Since the semiconductor NP-emission intensity depends on the distance from the NP, measuring the emission intensity allowed the determination of the local temperature within the NP's complex. Another quite simple method of measuring the metal NP temperature is a determination of the width (FWHM) of the SPR band in the absorption spectra of the NP. The resonance frequency of the SPR absorption band is also temperature-dependent, so
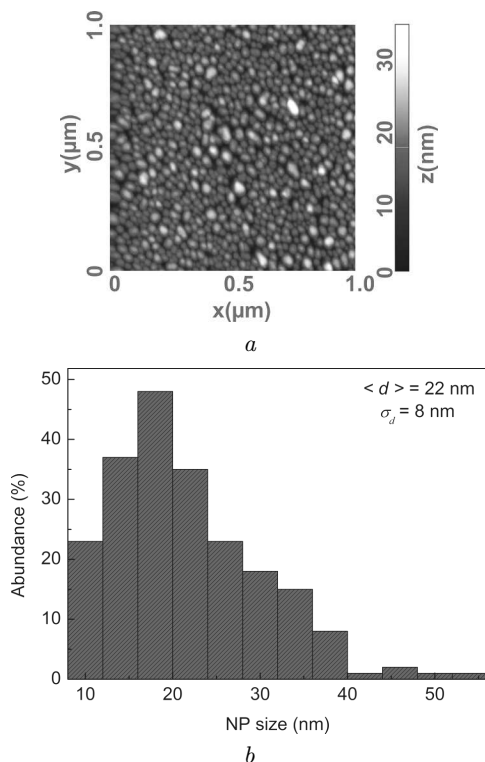
a

b

Fig. 16. AFM image of the Au NPs array on a glass substrate (*a*),lateral size distribution of Au NPs (*b*). (Modified from Ref. [105])
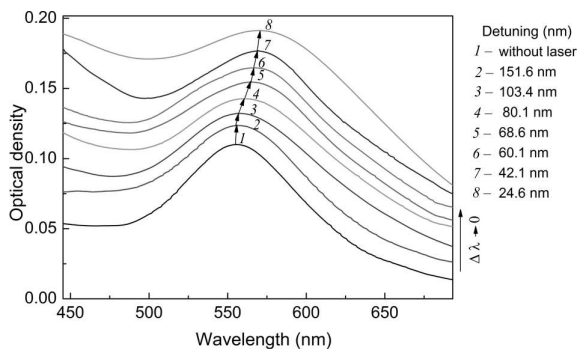

Fig. 17. Absorption spectra of the 2D array Au NPs without and under the simultaneous CW Ar$^+$ laser excitation with various wavelengths. Laser intensity is 5×10^3 W/cm^2. SPR wavelength for Au NPs without laser excitation is 556.6 nm. (Modified from Ref. [105])

knowledge of the temperature dependence of the SPR width and the resonance frequency allows one to determine the real temperature of the metal NP. The temperature dependence of the frequency and width of the SPR in metal NPs were reported in works

[29, 31–33, 37–39], where an appreciable red shift and a broadening of the SPR with increasing temperature were observed. The light-induced surface plasmon assisted heating of a dense 2D array of Au NPs [101] and Au NPs in colloids [102] was studied in our recent work, as described below.

3.2. Light-Induced Heating of a Dense 2D Monolayer of Au NPs

3.2.1. Experimental. Sample preparation and characterization

The sample of a dense 2D ensemble of Au NPs was prepared as follows. The Au film with a thickness of 5 nm was fabricated by the thermal vacuum deposition on a glass plate. The metal was vacuum-evaporated from simple sources, primarily from tungsten crucibles with shutters heated by an electric current. The crucibles were filled with a 99.99% purity metal Au, the pressure in the vacuum chamber was approximately 10^{-5} Torr, and the distance between the substrates and the filaments was 15 cm. Such a large distance between substrates and filaments allowed the production of uniform films. The thickness of the films was controlled both *in-situ*, via deposition monitors using quartz microbalances and by multiangle incident ellipsometry *ex-situ*. The Au film was then annealed at 370 °C for 30 min, leading to the transformation of the Au film to an ensemble of Au NPs.

The existence of Au NPs on a glass substrate was confirmed by AFM (Fig. 16) and by absorption spectra (Fig. 17). AFM measurements were performed with an NT-MDT Ntegra microscope in the semi-contact tapping mode, using Si cantilevers with a tip apex radius of 10 nm. The studied sample contained the Au NPs with a mean height of approximately 10 nm, while the mean lateral size was about 22 nm. Since, at optical measurements, the electric vector of incident light beams of an incandescent lamp and a laser were parallel to the Au NPs ensemble plane, only the lateral surface plasmon mode was excited in the NPs. Thus, only the lateral size distribution of the Au NPs was considered, a histogram of which is shown in Fig. 16, *b*. The size distribution parameters are as follows: the mean NP lateral size $\langle d \rangle = 22$ nm with a standard deviation of $\sigma_d = 8$ nm, and a mean interparticle distance $\langle D \rangle = 40$ nm with a standard deviation of $\sigma_D = 10$ nm.

A tungsten-halogen incandescent lamp served as a white light source for absorption measurements. Additional illumination of the Au NP ensemble was carried out by CW lasers with wavelengths of 660 nm, 532 nm, 514.5 nm, 496.5 nm, 488.0 nm, 476.5 nm, and 405.0 nm. The laser intensity in the excited spot on sample's surface was the same for each of the wavelengths and was 5×10^3 W/cm^2. The absorption spectra were measured at the normal incidence of the focused white light source on sample's surface (plane of the 2D Au NP ensemble). The incident angle of the focused laser beam was about 10^0, or almost the normal incidence, and the white light and laser beams were focused on the same point on sample's surface. A single-grating spectrometer MDR-3 was used for the registration of absorption spectra.

3.2.2. Results and discussion

Initially, the absorption spectrum of the 2D ensemble of Au NPs was measured without laser illumination, denoted by a black line in Fig. 17. The long wavelength band is the SPR band with a maximum at 556.6 nm. The short wavelength band corresponds to the interband absorption transitions in Au. The absorption spectra of Au NPs were then measured under the simultaneous CW laser excitation. The various laser wavelengths provide differing values of the detuning of the laser wavelength from the SPR. The absorption spectra are shown in Fig. 17. All of the spectra demonstrate the same two-band structure, and one can observe that approaching the SPR wavelength leads to a red shift and a broadening of the plasmonic band. A decrease of the laser detuning from the SPR leads to an increase in the intensity of the interband transition band.

For quantitative analysis of the absorption spectra and the dependence on the detuning, the measured spectra were fitted by basic Lorentz spectral bands. The fitting gives the width (FWHM), spectral position, and intensity of the SPR band. Figure 18 shows the dependences of the SPR broadening, spectral shift, and normalized intensity on the laser detuning from the SPR. The broadening is described by $\Delta\lambda(I)/\Delta\lambda_0$, where λ_0 is the SPR bandwidth without laser illumination, and $\Delta\lambda(I)$ is one at the laser illumination with intensity I. The spectral shift is $(\lambda_m(I) - \lambda_{m0})$, where λ_{m0} and $\lambda(I)$ are the SPR wavelengths without laser illumination and at the laser intensity I, respectively. The SPR band inten-
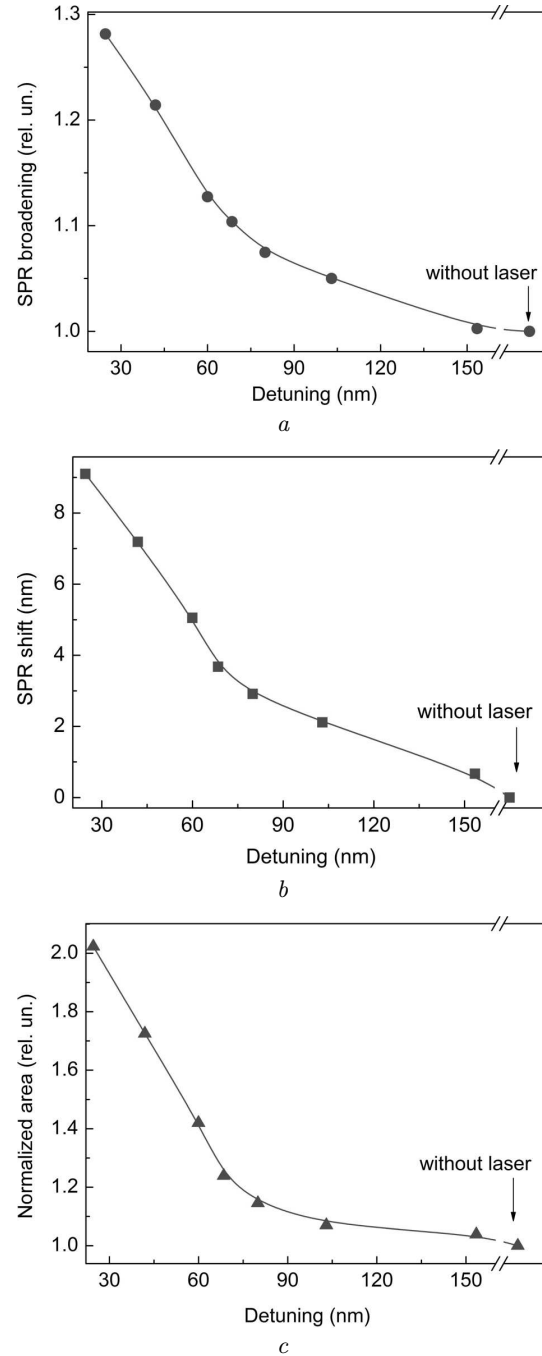

Fig. 18. Dependence of the SPR absorption band broadening (*a*), shift (*b*), and intensity (*c*) on the detuning of the laser excitation wavelength from the SPR. The values of the SPR band broadening, shift, and normalized intensity are taken with respect to SPR characteristics without laser excitation. Solid lines are the spline ones given to guide the eye. (Modified from Ref. [105])
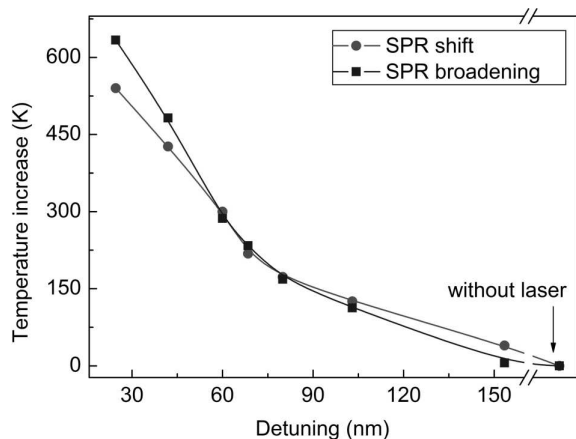
Fig. 19. Temperature of the 2D array of gold NPs versus the laser wavelength detuning from SPR estimated by the SPR shift (red circles) and the SPR bandwidth broadening (blue squares). Lines are the spline ones given to guide the eye. (Modified from Ref. [105])

sity is then normalized to the value obtained without laser illumination. Figures 17 and 18 show that, as the laser wavelength approaches the plasmon resonance, the SPR broadening occurs, along with a red shift and an increase in the intensity.

The SPR broadening (Fig. 18, *a*) reveals the Au NPs heating, due to the conversion of the free electron plasma oscillation energy to the thermal energy. Indeed, the rising temperature leads to an increase in the phonon population in the metal that, subsequently, leads to an increase in the rate of free electrons scattering on phonons. The temperature dependence of the electron-phonon scattering rate is discussed above and is given by Eq. (8). An increase in the scattering rate leads to a stronger plasmon damping and to an increase in the SPR bandwidth. When the laser wavelength approaches the SPR, the bandwidth increases proving the resonant plasmonic nature of the NP heating.

Additionally, when the laser wavelength approaches the SPR, an appreciable red shift of the plasmon band occurs. Like the SPR broadening, the red shift is the evidence of NP's heating. As we discussed in Section 1, the cause for such a shift is the thermal expansion of NPs. The thermal expansion leads to a decrease in the plasma bulk frequency and, in accordance with Eq. (12), to a decrease of the SPR frequency, ort the SPR red shift. Just as with the SPR broadening, when the laser wavelength approaches

the SPR, the plasmon band red shift increases proving the resonant plasmonic nature of the NP heating.

Consequently, approaching the SPR causes an increase in the amplitude of plasma oscillations and to the intensification of a heat generation by Au NPs. In our recent work [37], we measured the temperature dependence of the SPR red shift and the bandwidth broadening in spherical Au NPs of the same size (20 nm) as the NPs in the present sample; they were analyzed in the interval 290 to 1188 K. Thus, one can use the data on the temperature dependence of the SPR from Ref. [37] to estimate the temperature of Au NPs in the present experiments. The estimated temperature dependence of the Au NP ensemble on the laser detuning from the SPR is presented in Fig. 19. The red circles represent the dependence realized from the data on the SPR red shift, and the blue squares show the dependence obtained from the data on the SPR broadening. Both estimated dependences on the detuning are similar, and the estimated temperature values are quite close. This supports the correctness of our estimations of the temperature of the NPs. Strong heating occurs at a decrease in the laser detuning from the SPR. Indeed, the maximum temperature increase is about 590 K, with a minimal detuning of 24.6 nm. This resonant effect suggests that the surface plasmons play a significant role in the light-induced heating of metal NPs.

The strong heating of Au NPs in our experiments was achieved at a moderate CW laser intensity of 5×10^3 W/cm^2, so it may be due to a high concentration of Au NPs in the studied sample. As mentioned, the heating effect can be strongly enhanced in dense ensembles of NPs. There are two primary mechanisms of such increase in the heating; one is an accumulative effect, and another one is the plasmon coupling of NPs. The accumulative effect originates from an addition of heat fluxes generated by a single NP. The coupling effect is much more complicated. Interparticle coupling leads to a collectivization of plasmonic modes of individual NPs. The plasmon-enhanced electric field of such a coupled dense NP ensemble enhances the optical processes, including the light absorption by NPs. An increase in the absorption strengthens the NP heating.

Another interesting effect mentioned above is a noticeable increase in the intensity of the SPR absorption band, when the laser frequency approaches the SPR, see Figs. 17 and 18, *c*. At a minimal laser de-

tuning from the SPR, the intensity of the plasmonic band increases by 1.84 times with respect to the one without a laser. The decrease in the detuning of the laser from the SPR leads to a sufficient increase in the intensity of the short wavelength band corresponding to interband transitions in Au. As noted above, at the resonance of laser light with SPR, a strong enhancement of the local plasmonic field near the metal NP occurs. A sufficiently stronger plasmonic field arises in a dense ensemble of strongly interacting metal NPs. Thus, such a resonantly-generated plasmonic field enhances the processes of absorption and scattering of light by Au NPs, leading to an increase in the light absorption.

3.3. Light-Induced Heating of Au NPs in a Colloidal Solution

3.3.1. Experimental. Sample preparation and characterization

Au NPs were synthesized by a chemical reduction of the Au precursor ($HAuCl_4$) dissolved in a polymer aqueous solution. The polymer played the roles of nucleating, capping, and stabilizing agents simultaneously. Reduction of Ag salt was performed at $T = 5$ °C in aqueous solutions of Dextran-graft-Polyacrylamide copolymer (D-g-PAA). The D-g-PAA synthesis, polymer characterization, and peculiarities of their internal macromolecular structure were recently described in [103]. This copolymer possesses a star-like architecture, consisting of a compact dextran core and long Polyacrylamide arms. For D70-g-PAA employed in the present work, the conformation of PAA-grafts is extended and is locally worm-like. Due to a more compact molecular structure, the branched polymers have higher local concentrations of functional groups in comparison with linear Polyacrylamide. These structural peculiarities offer advantages for the application of branched polymer systems in nanotechnologies [104]. The pH value of the aqueous solutions of the polymer was 5.5, corresponding to the pH of deionized water. 0.012 ml of a 0.1 M $HAuCl_4$ aqueous solution was added to 0.5 ml of an aqueous polymer solution ($c = 1.1 \times 10^{-3}$ g/cm^3) and stirred for 20 min, and then 0.047 ml of a 0.1 M aqueous solution of $NaBH_4$ was added. The final aqueous solution was stirred for 30 min. The solution turned ruby-red in color, thus indicating the formation of Au NPs. *In situ* synthesis
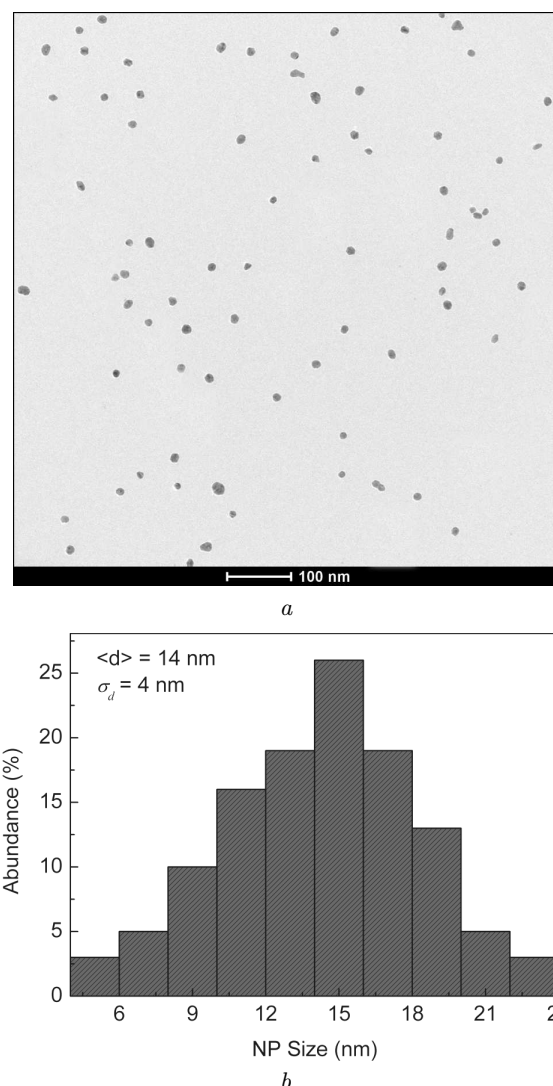
a

b

Fig. 20. TEM image (*a*) and the corresponding size distribution (*b*) of gold NPs in a colloid. (Modified from Ref. [106])

of Au NPs in dilute aqueous solutions of uncharged branched polymer matrices results in rather stable colloids.

Transmission electron microscopy (TEM) was used as a direct technique for the Au NP characterization. Observations of the Au NPs were carried out on two TEMs, Tecnai G2 or CM12 (FEI, Eindhoven Netherlands), and the images were acquired with a ss-CCD Eagle camera on the Tecnai and a Megaview SIS Camera on the CM12. The typical TEM image with a corresponding histogram of the size distribution for Au NPs is presented in Fig. 20. The characteristics of
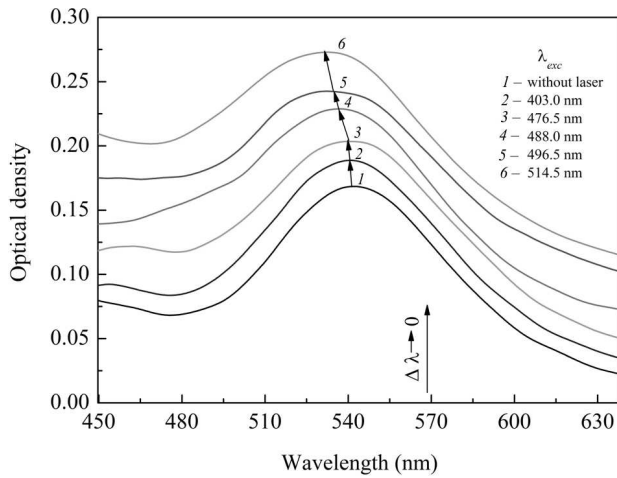
Fig. 21. Absorption spectra of Au NPs in colloid in a spectral range close to SPR without and under the simultaneous CW laser excitation with various wavelengths. Laser excitation intensity is 5×10^3 W/cm^2. SPR wavelength for Au NPs without laser excitation is 543 nm. (Modified from Ref. [106])

the size distribution are as follows: the mean size is $\langle d \rangle = 14$ nm with a standard deviation of $\sigma_d = 4$ nm.

3.3.2. Results and discussion

Initially, the absorption spectrum of colloidal Au NPs was measured without laser illumination. The respective spectrum is shown in Fig. 21 with a black line. The spectrum of Au NPs demonstrates the clear SPR band with a maximum at 543 nm. Then the absorption spectra of Au NPs were measured under the simultaneous laser illumination. We used the CW Ar$^+$ laser with wavelengths of 514.5 nm, 496.5 nm, 488.0 nm, and 476.5 nm, respectively, along with a diode laser with a wavelength of 403.0 nm. The various laser wavelengths provided the laser detuning from the SPR. The laser intensity was the same for all the wavelengths, remaining at 5×10^3 W/cm^2. The obtained absorption spectra are presented in Fig. 21. One can see that approaching the SPR wavelength leads to a blue shift and a broadening of the plasmonic band.

For the quantitative analysis of the absorption spectra in dependence on the detuning, the measured spectra were fitted by Lorentz spectral peaks as in the previous section. Again, the fitting gives the width (FWHM), spectral position, and intensity of the SPR band. Figure 22 presents the attained dependences of the SPR broadening, spectral shift,

and normalized intensity on the laser detuning from the SPR. As previously noted, the broadening is described by $\Delta\lambda(I)/\Delta\lambda_0$, where $\Delta\lambda_0$ is the SPR bandwidth without laser illumination and $\Delta\lambda(I)$ is the bandwidth at the laser illumination with intensity I. The spectral shift is $(\lambda_m(I) - \lambda_{m0})$, where λ_{m0} and $(\lambda_m(I)$ are the SPR wavelengths without laser illumination and at the laser intensity I, respectively. The SPR band intensity is normalized to that of the one obtained without laser illumination. Thus, one can see from Figs. 21 and 22 that approaching the laser wavelength to the plasmon resonance leads to the SPR broadening, a blue shift, and an increase in the intensity.

As noted, SPR broadening (Fig. 22, *a*) reveals the Au NP heating, due to the conversion of the energy of free electron plasma oscillations to the thermal energy. Heating leads to an increase in the phonon population in the metal, which leads to an increase in the rate of free electrons scattering on phonons. Again, the temperature dependence of the electron-phonon scattering rate is given above by Eq. (8). An increase in the scattering rate leads to a stronger plasmon damping and, correspondingly, to an increase in the SPR bandwidth. When the laser wavelength approaches the SPR, the bandwidth increases proving the resonant plasmonic nature of the NP heating. Approaching the SPR results in an increase in the amplitude of plasma oscillations and to the intensification of the heat generation by the Au NPs. The temperature dependence of the SPR broadening for spherical Au NPs with a size of 20 nm in the interval 290 to 1188 K was measured in Ref. [37]. Since the Au NPs analyzed herein were 14 nm, and close to the NPs in Ref. [37], one may use the data on the temperature dependence of the SPR broadening from Ref. [37] to estimate the temperature of Au NPs in the present experiments. The estimated dependence of the Au NP temperature on the laser detuning is presented in Fig. 23, with the estimation of a strong increase of 316 K at a minimal detuning of 28.5 nm. This is suggestive of the significant role of surface plasmons in light-induced heating of metal NPs.

From Fig. 22, *b*, one can see that when the laser wavelength approaches the plasmon resonance, it leads to the SPR blue shift. At the laser detuning higher than 68 nm, the SPR blue shift with decreasing detuning is quite small (about –0.7 nm). Meanwhile, at a detuning lower than 68 nm, a sharp in-

crease in the SPR blue shift occurs (−8.3 nm at a detuning of 28.5 nm). Let us consider the origin of such shift, given our previous theoretical calculations. According to Eq. (6), the SPR frequency ω_{sp} in metal NPs depends on the bulk plasma frequency ω_p, the contribution of bound electrons in the permittivity of the metal ε_b, and the permittivity of the environment ε_m. Thus, the SPR frequency ω_{sp} can be temperature-dependent through the respective dependence of ω_p, ε_b, and ε_m. As we note above in Eq. (11), – temperature increase results in a decrease in the bulk plasma frequency ω_p, caused by the thermal expansion of the NPs. Therefore, the thermal expansion should lead to a decrease in the bulk plasma frequency and, in accordance with Eq. (6), to a decrease in the SPR frequency or to the SPR red shift. However, in our experiments, we observed a blue shift instead of a red one. Taking into account the slight temperature dependence of the contribution of bound electrons in the permittivity of Au, or ε_b from Ref. [105], it is reasonable to assume that the cause for the SPR blue shift is the temperature dependence of the permittivity of the environment ε_m. Indeed, the permittivity of water decreases with rising temperature [106], causing a SPR blue shift in accordance with Eq. (6). However, a decrease in the water permittivity is quite slight, and it decreases from 1.7764 at 20 °C to 1.7496 at 90 °C. Both values are taken from Ref. [106] for a wavelength of 589 nm, which is close to the SPR wavelength for the studied sample at the normal pressure. Considering such a slight temperature-induced decrease in the water permittivity and the competitive red shift of the SPR originating from the NP thermal expansion, the SPR blue shift should be small at a slight NP heating, occurring at the laser detuning higher than 68 nm, as shown in Fig. 23.

At detuning values lower than 68 nm, the SPR blue shift increases sharply, as shown in Fig. 22, *b*. From Fig. 23, one observes that, at detuning values lower than 68 nm, the NP temperature exceeds the boiling point of water. Thus, at a detuning lower than 68 nm, the water boiling should lead to the formation of vapor bubbles around the excited NPs. The dielectric permittivity of vapor (1.0005) is considerably lower than that of water (1.7496) [106], where both values are given for temperatures of 100 °C and 90 °C, respectively. Thus, the formation of vapor bubbles around the Au NPs should lead to a sharp
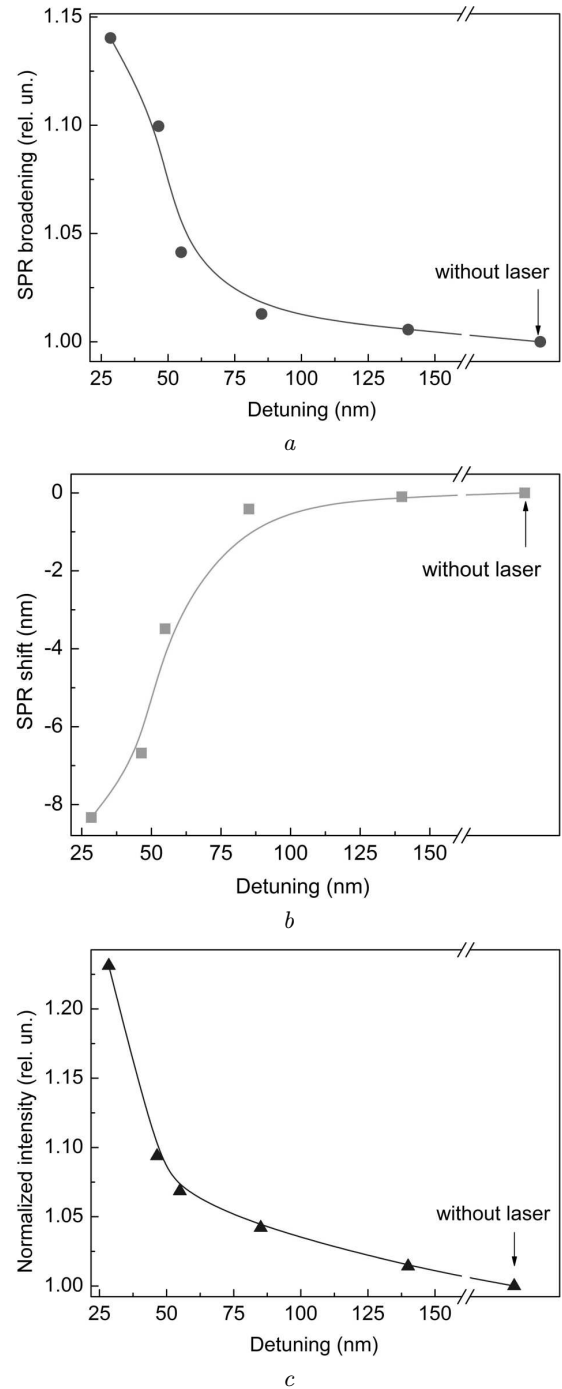

Fig. 22. Dependence of the SPR absorption band broadening (*a*), shift (*b*), and intensity (*c*) on the detuning of the laser wavelength from SPR. The values of the SPR band broadening, shift, and normalized intensity are given relative to SPR ones obtained without laser illumination. Solid lines are the spline ones given to guide the eye. (Modified from Ref. [106])
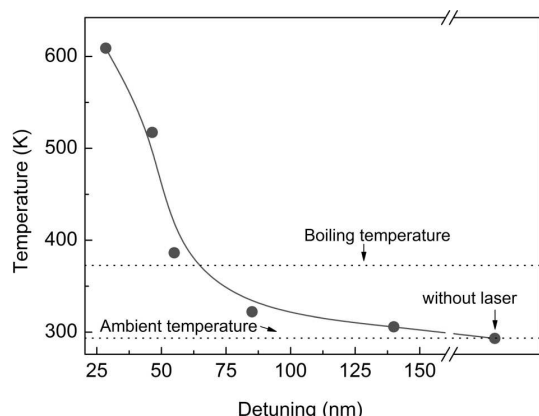
Fig. 23. Temperature of the gold NPs versus the laser wavelength detuning from SPR estimated by the SPR broadening (circles). Solid line is the spline one given to guide the eye. (Modified from Ref. [106])

blue shift of the SPR in accordance with Eq. (6). This supports our observation, which is in full agreement with the observation of Ref. [84], where an appreciable SPR blue shift was observed at the vapor bubble formation around the Au NPs, as seen in Fig. 22. The sharp blue shift of the SPR at temperatures higher than the water boiling point is likely due to the vapor-bubble formation around the Au NPs. At a decrease in the detuning and the resulting temperature increase, the bubble size increases. Subsequently, the dielectric permittivity of NP's environment decreases causing an increase in the SPR blue shift in accordance with Eq. (6).

Another interesting effect mentioned above is the noticeable increase in the intensity of the SPR absorption band, as the laser frequency approaches the SPR, Fig. 22, *c*. At the minimal laser detuning from the SPR, the intensity of the plasmonic band increases by 1.23 times with respect to the one without the laser. The nature of such resonant effect should be clarified: at the resonance of laser light with SPR, the strong increase in the magnitude of plasma oscillations occurs, resulting in the strong increase in the local plasmonic field near the metal NP. Such ag strong local field greatly enhances the optical processes such as the surface enhanced Raman scattering (SERS), surface enhanced photoluminescence (SEPL), and surface enhanced absorption in molecules and clusters located near the surface of metal NPs, as well as within the metal NPs. One can hypothesize that a resonantly generated plasmonic field enhances the process of light absorption by Au NPs, leading to an increase in the absorption band intensity.

3.4. Conclusions

The surface-plasmon-involved laser heating of a dense 2D ensemble of Au NPs and Au NPs in water colloids was studied. The CW lasers with various wavelengths and an intensity of 5×10^3 W/cm^2 were used for the Au NP illumination. Along with the laser illumination, the absorption spectra of Au NPs were measured simultaneously, and we found that the temperature of Au NPs has a strong dependence on the laser frequency detuning from the SPR in Au NPs. For example, the temperature increases, when the laser frequency approaches the SPR, and the heating displayed a resonant character.

Strong heating in a dense 2D ensemble of Au NPs up to 590 K was observed at a moderate excitation intensity of 5×10^3 W/cm^2 and a detuning of 24.6 nm. Such strong heating is likely due to the accumulative effects of the light absorption enhancement by an intense local plasmonic field of coupled Au NPs within the aforementioned 2D ensemble.

The strong increase in the temperature of Au NPs in a water colloid of 316 K was obtained at the moderate laser intensity of 5×10^3 W/cm^2 and a detuning of 28.5 nm. The SPR blue shift was observed, when the laser frequency approached the SPR. The SPR blue shift increased sharply, when the NP temperature exceeded the water boiling point, likely due to vapor bubbles generated near the surface of Au NPs.

1. A. Barhoumi, D. Zhang, F. Tam, N. Halas. Surface-enhanced Raman spectroscopy of DNA. *J. Am. Chem. Soc.* **130**, 5523 (2008).
2. F. Le, D. Brandl, Y. Urzhumov, H. Wang, J. Kundu, N. Halas, J. Aizpurua, P. Nordlander. Metallic NP arrays: A common substrate for both surface-enhanced Raman scattering and surface-enhanced infrared absorption. *ACS Nano* **2**, 707 (2008).
3. G. Laurent, N. Felidj, J. Grand, J. Aubard, G. Levi, A. Hohenau, J. Krenn, F. Aussenegg. Probing surface plasmon fields by far-field Raman imaging. *J. Microscopy* **229**, 189 (2008).

4. R. Bakker, H. Yuan, Z. Liu, V. Drachev, A. Kildishev, V. Shalaev, R. Pedersen, S. Gresillon, A. Boltasseva. Enhanced localized fluorescence in plasmonic nanoantennae. *Appl. Phys. Lett.* **92**, 043101 (2008).

5. G. Gay, B. de Lesegno, R. Mathevet, J. Weiner, H. Lezec, T. Ebbesen. Atomic fluorescence mapping of optical field intensity profiles issuing from nanostructured slits, milled into subwavelength metallic layers. *Appl. Phys. B* **81**, 871 (2005).

6. O.A. Yeshchenko, I.M. Dmitruk, A.A. Alexeenko, M.Yu. Losytskyy, A.V. Kotko, A.O. Pinchuk. Size-dependent surface-plasmon-enhanced photoluminescence from silver nanoparticles embedded in silica. *Phys. Rev. B* **79**, 235438 (2009).

7. A. Gobin, M. Lee, R. Drezek, N. Halas, J. West. Vascular targeting of nanoshells for photothermal cancer therapy. *Clin. Cancer Res.* **12**, B83 (2014).

8. C. Hubert, A. Rumyantseva, G. Lerondel, J. Grand, S. Kostcheev, L. Billot, A. Vial, R. Bachelot, P. Royer. Near-field photochemical imaging of noble metal nanostructures. *Nano Lett.* **5**, 615 (2005).

9. K. Kandere-Grzybowska, C. Campbell, Y. Komarova, B. Grzybowski, G. Borisy. Molecular dynamics imaging in micropatterned living cells. *Nature Methods* **2**, 739 (2005).

10. M. Choi, K.J. Stanton-Maxey, J.K. Stanley, C.S. Levin, R. Bardhan, D. Akin, S. Badve, J. Sturgis, J.P. Robinson, R. Bashir, N.J. Halas, S.E. Clare. A cellular trojan horse for delivery of therapeutic nanoparticles into tumors. *Nano Lett.* **7**, 3759 (2007).

11. L. Hirsch, A. Gobin, A. Lowery, F. Tam, R. Drezek, N. Halas, J. West. Metal nanoshells. *Ann. Biomed. Engin.* **34**, 15 (2006).

12. D. O'Neal, L. Hirsch, N. Halas, J. Payne, J. West. Photothermal tumor ablation in mice using near infrared-absorbing nanoparticles. *Cancer Lett.* **209**, 171 (2004).

13. D. Citrin. Plasmon polaritons in finite-length metal-nanoparticle chains: the role of chain length unravelled. *Nano Lett.* **5**, 985 (2005).

14. J. Jung, T. Sondergaard, S. Bozhevolnyi. Theoretical analysis of square surface plasmon-polariton waveguides for long-range polarization-independent waveguiding. *Phys. Rev. B* **76**, 035434 (2007).

15. K. Leosson, T. Nikolajsen, A. Boltasseva, S. Bozhevolnyi. Long-range surface plasmon polariton nanowire waveguides for device applications. *Opt. Express* **14**, 314 (2006).

16. B. Steinberger, A. Hohenau, H. Ditlbacher, A. Stepanov, A. Drezet, F. Aussenegg, A. Leitner, J. Krenn. Dielectric stripes on gold as surface plasmon waveguides. *App. Phys. Lett.* **88**, 094104 (2006).

17. J. Takahara, S. Yamagishi, H. Taki, A. Morimoto, T. Kobayashi. Guiding of a one-dimensional optical beam with nanometer diameter. *Opt. Lett.* **22**, 475 (1997).

18. U. Kreibig, M. Vollmer. Optical Properties of Metal Clusters (Springer, 1995) [ISBN: 978-3-662-09109-8].

19. C.F. Bohren, D.R. Huffman. *Absorption and Scattering of Light by Small Particle* (Wiley, 1998) [ISBN: 9783527618156].

20. B.G. Ershov, E. Janata, A. Henglein, A. Fojtik. Silver atoms and clusters in aqueous solution: Absorption spectra and the particle growth in the absence of stabilizing $Ag+$ ions. *J. Phys. Chem.* **97**, 4589 (1993).

21. A. Henglein. Physicochemical properties of small metal particles in solution: "microelectrode" reactions, chemisorption, composite metal particles, and the atom-to-metal transition. *J. Phys. Chem.* **97**, 5457 (1993).

22. U. Kreibig. Interface-induced dephasing of Mie plasmon polaritons. *Appl. Phys. B* **93**, 79 (2008).

23. W.A. Challener, C. Peng, A.V. Itagi, D. Karns, W. Peng, Y. Peng, X.M. Yang, X. Zhu, N.J. Gokemeijer, Y.-T. Hsia, G. Ju, R.E. Rottmayer, M.A. Seigler, E.C. Gage. Heat-assisted magnetic recording by a near-field transducer with efficient optical energy transfer. *Nature Photon.* **3**, 220 (2009).

24. L.R. Hirsch, R.J. Stafford, J.A. Bankson, S.R. Sershen, B. Rivera, R.E. Price, J.D. Hazle, N.J. Halas, J.L. West. Nanoshell-mediated near-infrared thermal therapy of tumors under magnetic resonance guidance. *Proc. Natl. Acad. Sci. USA* **100**, 13549 (2003).

25. A. Lowery, A. Gobin, E. Day, N. Halas, J. West. Immunonanoshell laser-assisted therapy targets and ablates tumor cells. *Breast Cancer Res. Treat.* **100**, S289 (2006).

26. A. Lowery, A. Gobin, E. Day, N. Halas, J. West. Immuno nanoshells for targeted photothermal ablation of tumor cells. *Int. J. Nanomed.* **1**, 149 (2006).

27. L. Cao, D.N. Barsic, A.R. Guichard, M.L. Brongersma. Plasmon-assisted local temperature control to pattern individual semiconductor nanowires and carbon nanotubes. *Nano Lett.* **7**, 3523 (2007).

28. W. Cai, J.S. White, M.L. Brongersma. Compact, hight-speed and power-efficient electrooptic plasmonic modulators. *Nano Lett.* **9**, 4403 (2009).

29. U. Kreibig. Electronic properties of small silver particles: the optical constants and their temperature dependence. *J. Phys. F* **4**, 999 (1974).

30. R.H. Doremus. Optical properties of small gold particles. *J. Chem. Phys.* **40**, 2389 (1964).

31. R.H. Doremus. Optical properties of small silver particles. *J. Chem. Phys.* **42**, 414 (1965).

32. P. Mulvaney. *Nanoscale Materials in Chemistry.* Edited by K.J. Klabunde (Wiley, 2001), P. 121.

33. J.-S.G. Bouillard, W. Dickson, D.P. O'Connor, G.A. Wurtz, A.V. Zayats. Low-temperature plasmonics of metallic nanostructures. *Nano Lett.* **12**, 1561 (2012).

34. D.Yu. Fedyanin, A.V. Krasavin, A.V. Arsenin, A.V. Zayats. Surface plasmon polariton amplification upon electrical injection in highly integrated plasmonic circuits. *Nano Lett.* **12**, 2459 (2012).

35. S. Link, M.A. El-Sayed. Size and temperature dependence of the plasmon absorption of colloidal gold nanoparticles. *J. Phys. Chem. B* **103**, 4212 (1999).

36. O.A. Yeshchenko, I.M. Dmitruk, A.A. Alexeenko, A.V. Kotko, J. Verdal, A.O. Pinchuk. Size and temperature effects on the surface plasmon resonance in silver nanoparticles. *Plasmonics* **7**, 685 (2012).

37. O.A. Yeshchenko, I.S. Bondarchuk, V.S. Gurin, I.M. Dmitruk, A.V. Kotko. Temperature dependence of the surface plasmon resonance in gold nanoparticles. *Surf. Sci.* **608**, 275 (2013).

38. O.A. Yeshchenko, I.S. Bondarchuk, A.A. Alexeenko, A.V. Kotko. Temperature dependence of the surface plasmon resonance in silver nanoparticles. *Functional Materials* **20**, 357 (2013).

39. O.A. Yeshchenko. Temperature effects on the surface plasmon resonance in copper nanoparticles. *Ukr. J. Phys.* **58**, 249 (2013).

40. O.A. Yeshchenko, I.M. Dmitruk, A.M. Dmytruk, A.A. Alexeenko. Influence of annealing conditions on size and optical properties of copper nanoparticles embedded in silica matrix. *Mater. Sci. Eng. B* **137**, 247 (2007).

41. O.A. Yeshchenko, I.M. Dmitruk, A.A. Alexeenko, A.M. Dmytruk. Size-dependent melting of spherical copper nanoparticles embedded in a silica matrix. *Phys. Rev. B* **75**, 085434 (2007).

42. V.S. Gurin, A.A. Alexeenko, K.V. Yumashev, P.V. Prokoshin, S.A. Zolotovskaya, G.A. Zhavnerko. Structure and optical properties of CuxO- and CuxSe-doped sol-gel silica glasses. *Mater. Sci. Eng. C* **23**, 1063 (2003).

43. U. Kreibig, L. Genzel. Optical absorption of small metallic particles. *Surf. Sci.* **156**, 678 (1985).

44. S. Link, M. El-Sayed. Size and temperature dependence of the plasmon absorption of colloidal gold nanoparticles. *J. Phys. Chem. B* **103**, 4212 (1999).

45. N.I. Grigorchuk, P.M. Tomchuk. Optical and transport properties of spheroidal metal nanoparticles with account for the surface effect. *Phys. Rev. B* **84**, 085448 (2011).

46. K. Ujihara. Reflectivity of metals at high temperatures. *J Appl. Phys.* **43**, 2376 (1972).

47. R.H. Bube. *Electrons in Solids: An Introductory Survey* (Academic Press, 1992) [ISBN: 9780080505381].

48. Z. Li-Jun, G. Jian-Gang, Z. Ya-Pu. Size- and temperature-dependent thermal expansion coefficient of a nanofilm. *Chin. Phys. Lett.* **26**, 066201 (2009).

49. J.H. Wray, J.T. Neu. Refractive index of several glasses as a function of wavelength and temperature. *J. Opt. Soc. Am.* **59**, 774 (1969).

50. P.B. Johnson, R.W. Christy. Optical constants of noble metals. *Phys. Rev. B* **6**, 4370 (1972).

51. N.W. Ashcroft, N.D. Mermin. *Solid State Physics* (Saunders College, 1976) [ISBN: 0030839939].

52. R.C. Lincoln, K.M. Koliwad, P.B. Ghate. Morse-potential evalution of second- and third-order elastic constants of some cubic metals. *Phys. Rev.* **157**, 463 (1967).

53. O.A. Yeshchenko, I.M. Dmitruk, K.P. Grytsenko, V.M. Prokopets, A.V. Kotko, S. Schrader. Influence of interparticle interaction on melting of gold nanoparticles in Au/polytetrafluoroethylene nanocomposites. *J. Appl. Phys.* **105**, 094326 (2009).

54. O.A. Yeshchenko, I.M. Dmitruk, A.A. Alexeenko, A.V. Kotko. Surface plasmon as a probe for melting of silver nanoparticles. *Nanotechnology* **21**, 045203 (2010).

55. M. Schwind, V.P. Zhdanov, I. Zoric, B. Kasemo. LSPR study of the kinetics of the liquid-solid phase transition in Sn nanoparticles. *Nano Lett.* **10**, 931 (2010).

56. C. Kittel. *Introduction to Solid State Physics* (Willey, 2005) [ISBN: 978-0-471-41526-8].

57. A. Mooradian. Photoluminescence of metals. *Phys. Rev. Lett.* **22**, 185 (1969).

58. S.W. Chen, R.S. Ingram, M.J. Hostetler, J.J. Pietron, R.W. Murray, T.G. Schaaff, J.T. Khoury, M.M. Alvarez, R.L. Whetten. Gold nanoelectrodes of varied size: transition to molecule-like charging. *Science* **280**, 2098 (1998).

59. R.S. Ingram, M.J. Hostetler, R.W. Murray, T.G. Schaaff, J.T. Khoury, R.L. Whetten, T.P. Bigioni, D.K. Guthrie, P.N. First. 28 kDa alkanethiolate-protected Au clusters give analogous solution electrochemistry and STM coulomb staircases. *J. Am. Chem. Soc.* **119**, 9279 (1997).

60. P. Apell, R. Monreal, S. Lundqvist. Photoluminescence of noble metals. *Phys. Scr.* **38**, 174 (1988).

61. W. Knoll, M.R. Philpott, J.D. Swalen, A. Girlando. Emission of light from Ag metal gratings coated with dye monolayer assemblies. *J. Chem. Phys.* **75**, 4795 (1981).

62. O.A. Yeshchenko, I.M. Dmitruk, A.A. Alexeenko, M.Yu. Losytskyy, A.V. Kotko, A.O. Pinchuk. Size-dependent surface-plasmon-enhanced photoluminescence from silver nanoparticles embedded in silica. *Phys. Rev. B* **79**, 235438 (2009).

63. A.P. Zhang, J.Z. Zhang, Y. Fang. Photoluminescence from colloidal silver nanoparticles. *J. Lumin.* **128**, 1635 (2008).

64. O. Veron, J.P. Blondeau, N. Abdelkrim, E. Ntsoenzok. Luminescence study of silver nanoparticles obtained by annealed ionic exchange silicate glasses. *Plasmonics* **5**, 213 (2010).

65. O.A. Yeshchenko, I.S. Bondarchuk, M.Yu. Losytskyy, A.A. Alexeenko. Temperature dependence of photoluminescence from silver nanoparticles. *Plasmonics* **9**, 93 (2014).

66. J.P. Wilcoxon, J.E. Martin, F. Parsapour, B. Wiedenman, D.F. Kelley. Photoluminescence from nanosize gold clusters. *J. Chem. Phys.* **108**, 9137 (1998).

67. M.B. Mohamed, V. Volkov, S. Link, M.A. El-Sayed. The "lightning" gold nanorods: Fluorescence enhancement of over a million compared to the gold metal. *Chem. Phys. Lett.* **317**, 517 (2000).

68. O.A. Yeshchenko, I.S. Bondarchuk, M.Yu. Losytskyy. Surface plasmon enhanced photoluminescence from copper nanoparticles: influence of temperature. *J. Appl. Phys.* **116**, 054309 (2014).

69. Q. Darugar, W. Qian, M.A. El-Sayed, M.P. Pileni. Size-dependent ultrafast electronic energy relaxation and en-

hanced fluorescence of copper nanoparticles. *J. Phys. Chem. B* **110**, 143 (2006).

70. G.T. Boyd, Z.H. Yu, Y.R. Shen. Photoinduced luminescence from the noble metals and its enhancement on roughened surfaces. *Phys. Rev. B* **33**, 7923 (1986).

71. F. Hubenthal. Increased damping of plasmon resonances in gold nanoparticles due to broadening of the band structure. *Plasmonics* **8**, 1341 (2013).

72. D.J. Whittle, E. Burstein. Raman-scattering by resonant molecules at smooth metal-surfaces. *Bull. Am. Phys. Soc.* **26**, 777 (1981).

73. F.T. Xie, H.Y. Bie, L.M. Duan, G.H. Li, X. Zhang, J.Q. Xu. Self-assembly of silver polymers based on flexible isonicotinate ligand at different pH values: syntheses, structures and photoluminescent properties. *J. Solid State Chem.* **178**, 2858 (2005).

74. O.A. Yeshchenko, S.V. Kondratenko, V.V. Kozachenko. Surface plasmon enhanced photoluminescence from fullerene C60 film on Au nanoparticles array: resonant dependence on excitation frequency. *J. Appl. Phys.* **111**, 124327 (2012).

75. A.V. Akimov, A. Mukherjee, C.L. Yu, D.E. Chang, A.S. Zibrov, P.R. Hemmer, H. Park, M.D. Lukin. Generation of single optical plasmons in metallic nanowires coupled to quantum dots. *Nature* **450**, 402 (2007).

76. S. Garg, B. Singh, X. Liu, A. Jain, N. Ravishankar, L. Interrante, G. Ramanath. Metal-dielectric interface toughening by catalyzed ring opening in a monolayer. *J. Phys. Chem. Lett.* **1**, 336 (2010).

77. S. Garg, A. Jain, C. Karthik, B. Singh, R. Teki, V.S. Smentkowski, M.W. Lane, G. Ramanath. Metal-dielectric interface toughening by molecular nanolayer decomposition. *J. Appl. Phys.* **108**, 034317 (2010).

78. D.A. Zatsepin, V.S. Kortov, E.Z. Kurmaev, N.V. Gavrilov, R.G. Wilks, A. Moewes. X-ray emission and photoluminescence spectroscopy of nanostructured silica with implanted copper ions. *Phys. Solid State* **50**, 2322 (2008).

79. D. Dalacu, M. Martinu. Optical properties of discontinuous gold films: finite-size effects. *J. Opt. Soc. Am. B* **18**, 85 (2001).

80. O.A. Yeshchenko, I.S. Bondarchuk, V.V. Kozachenko, M.Yu. Losytskyy. Photoluminescence of rhodamine 6G in plasmonic field of Au nanoparticles: temperature effects. *J. Lumin.* **158**, 294 (2015).

81. O.A. Yeshchenko, I.S. Bondarchuk, V.V. Kozachenko, M.Yu. Losytskyy. Sensing the temperature influence on plasmonic field of metal nanoparticles by photoluminescence of fullerene C60 in layered C60/Au system. *J. Appl. Phys.* **117**, 153102 (2015).

82. A.O. Govorov, W. Zhang, T. Skeini, H. Richardson, J. Lee, N.A. Kotov. Gold nanoparticle ensembles as heaters and actuators: melting and collective plasmon resonances. *Nanoscale Res. Lett.* **1**, 84 (2006).

83. A.O. Govorov, H.H. Richardson. Generating heat with metal nanoparticles. *Nano Today* **2**, 30 (2007).

84. Z. Fang, Y.R. Zhen, O. Neumann, A. Polman, F.J. Garcia de Abajo, P. Nordlander, N.J. Halas. Evolution of light-induced vapor generation at a liquid-immersed metallic nanoparticle. *Nano Lett.* **13**, 1736 (2013).

85. B. Choudhuri, A. Mondal, J.C. Dhar, N.K. Singh, T. Goswami, K.K. Chattopadhyay. Enhanced photocurrent from generated photothermal heat in indium nanoparticles embedded TiO2 film. *Appl. Phys. Lett.* **102**, 233108 (2013).

86. H.A. Atwater, A. Polman. Plasmonics for improved photovoltaic devices. *Nature Mater.* **9**, 205 (2010).

87. D. Erickson, D. Sinton, D. Psaltis. Optofluidics for energy applications. *Nature Photonics* **5**, 583 (2011).

88. J.A. Schuller, T. Taubner, M.L. Brongersma. Optical antenna thermal emitters. *Nature Photonics* **3**, 658 (2009).

89. J.R. Adleman, D.A. Boyd, D.G. Goodwin, D. Psaltis. Heterogenous catalysis mediated by plasmon heating. *Nano Lett.* **9**, 4417 (2009).

90. P. Christopher, H.L. Xin, S. Linic. Visible-light-enhanced catalytic oxidation reactions on plasmonic silver nanostructures. *Nature Chem.* **3**, 467 (2011).

91. S. Ibrahimkutty, J. Kim, M. Cammarata, F. Ewald, J. Choi, H. Ihee, A. Plech. Ultrafast structural dynamics of the photocleavage of protein hybrid nanoparticles. *ACS Nano* **5**, 3788 (2011).

92. J. Lee, A.O. Govorov, N.A. Kotov. Nanoparticle assemblies with molecular springs: a nanoscale thermometer. *Angew. Chem. Int. Ed.* **44**, 7439 (2005).

93. Z.Z.J. Lim, J.E.J. Li, C.T. Ng, L.Y.L. Yung, B.H. Bay. Gold nanoparticles in cancer therapy. *Acta Pharmacol. Sin.* **32**, 983 (2011).

94. G. von Maltzahn, J.-H. Park, K.Y. Lin, N. Singh, C. Schwoppe, R. Mesters, W.E. Berdel, E. Ruoslahti, M.J. Sailor, S.N. Bhatia. Nanoparticles that communicate in vivo to amplify tumour targeting. *Nature Mater.* **10**, 545 (2011).

95. J.R. Adleman, D.A. Boyd, D.G. Goodwin, D. Psaltis. Heterogenous catalysis mediated by plasmon heating. *Nano Lett.* **9**, 4417 (2009).

96. D.A. Boyd, L. Greengard, L. Brongersma, M.Y. El-Naggar, D.G. Goodwin. Plasmon-assisted chemical vapor deposition. *Nano Lett.* **6**, 2592 (2006).

97. C. Li, Z. Wang, P.I. Wang, Y. Peles, N. Koratkar, G.P. Peterson. Nanostructured copper interfaces for enhanced boiling. *Small* **4**, 1084 (2008).

98. H.H. Richardson, M.T. Carlson, P.J. Tandler, P. Hernandez, A.O. Govorov. Experimental and theoretical studies of light-to-heat conversion and collective heating effects in metal nanoparticle solutions. *Nano Lett.* **9**, 1139 (2009).

99. M.T. Carlson, A.J. Green, H.H. Richardson. Superheating water by CW excitation of gold nanodots. *Nano Lett.* **12**, 1534 (2012).

100. E. Lukianova-Hleb, Y. Hu, L. Latterini, L. Tarpani, S. Lee, R.A. Drezek, J.H. Hafner, D.O. Lapotko. Plasmonic nanobubbles as transient vapor nanobubbles generated around plasmonic nanoparticles. *ACS Nano* **4**, 2109 (2010).

101. O.A. Yeshchenko, V.V. Kozachenko. Light-induced heating of dense 2D ensemble of gold nanoparticles: dependence on detuning from surface plasmon resonance. *J. Nanopart. Res.* **17**, 296 (2015).

102. O.A. Yeshchenko, N.V. Kutsevol, A.P. Naumenko. Light-induced heating of gold nanoparticles in colloidal solution: dependence on detuning from surface plasmon resonance. *Plasmonics* **11**, 345 (2016).

103. N. Kutsevol, T. Bezugla, M. Bezuglyi, M. Rawiso. Star-like dextran-graft-(polyacrylamide-copolyacrylic acid) copolymers. *Macromol Symp.* **82**, 317 (2012).

104. V. Chumachenko, N. Kutsevol, M. Rawiso, M. Schmutz, C. Blanck. In situ formation of silver nanoparticles in linear and branched polyelectrolyte matrices using various reducing agents. *Nanoscale Res. Lett.* **9**, 164 (2014).

105. Y.-J. Chen, M.-C. Lee, C.-M. Wang. Dielectric function dependence on temperature for Au and Ag. *Japan J. Appl. Phys.* **53**, 08MG02 (2014).

106. I. Thormahlen, J. Straub, U. Grigull. Refractive index of water and its dependence on wavelength, temperature, and density. *J. Phys. Chem. Refer. Data* **14**, 933 (1985).

O.A. Єщенко, А.О. Пінчук

ТЕРМО-ОПТИЧНІ ЕФЕКТИ
В ПЛАЗМОННИХ МЕТАЛЕВИХ НАНОСТРУКТУРАХ

Представлено огляд ефектів, пов'язаних із впливом температури на поверхневий плазмонний резонанс (ППР) в наночастинках благородних металів у діапазоні 77–1190 K. Виявлено, що підвищення температури приводить до помітного червоного зсуву, а також – до розширення ППР у наночастинках (НЧ). Показано, що теплове розширення та збільшення частоти електрон-фононного розсіяння, що відбуваються при збільшенні температури, є домінуючими фізичними механізмами, що приводять до червоного зсуву та розширення ППР. Виявлено ефект сильної температурної залежності, підсиленої поверхневими плазмонами фотолюмінесценції наночастинок срібла (Ag) та міді (Cu). Квантовий вихід фотолюмінесценції наночастинок Ag зменшується при підвищенні температури внаслідок зменшення фактора плазмонного підсилення, зумовленого збільшенням частоти електрон-фононного розсіяння. У той же час, було виявлено аномальну залежність від температури фотолюмінесценції наночастинок Cu, а саме – збільшення квантового виходу фотолюмінесценції зі збільшенням температури. Показано, що спільний вплив ППР та міжзонних переходів відіграє визначальну роль у цьому ефекті. Досліджено також зумовлений поверхневими плазмонами лазерний нагрів щільного 2D-масиву наночастинок Au на діелектричній підкладинці та наночастинок Au у водних колоїдних розчинах. Показано, що наближення частоти лазера до ППР приводить до сильного нагріву наночастинок Au. Такий резонансний ефект доводить плазмонний характер лазерного нагріву металевих НЧ. Спостережуваний різкий блакитний зсув поверхневого плазмонного резонансу в НЧ Au в колоїдному розчині при температурах, що перевищують температуру кипіння води, свідчить про утворення локальних нанорозмірних бульбашок водяної пари навколо наночастинок.

К л ю ч о в і   с л о в а: металеві наночастинки, поверхневий плазмонний резонанс, температурні ефекти, електрон-фононне розсіяння, теплове розширення наночастинки, плазмонна фотолюмінесценція, нагрівання світлом.